Constraints on Black Hole Spin in a Sample of Broad Iron Line AGN

Laura W. Brenneman[1], Christopher S. Reynolds[2]

ABSTRACT

We present a uniform X-ray spectral analysis of nine type-1 active galactic nuclei (AGN) that have been previously found to harbor relativistically broadened iron emission lines. We show that the need for relativistic effects in the spectrum is robust even when one includes continuum "reflection" from the accretion disk. We then proceed to model these relativistic effects in order to constrain the spin of the supermassive black holes in these AGN. Our principal assumption, supported by recent simulations of geometrically-thin accretion disks, is that no iron line emission (or any associated X-ray reflection features) can originate from the disk within the innermost stable circular orbit. Under this assumption, which tends to lead to constraints in the form of lower limits on the spin parameter, we obtain non-trivial spin constraints on five AGN. The spin parameters of these sources range from moderate ($a \sim 0.6$) to high ($a > 0.96$). Our results allow, for the first time, an observational constraint on the spin distribution function of local supermassive black holes. Parameterizing this as a power-law in dimensionless spin parameter ($f(a) \propto |a|^{\zeta}$), we present the probability distribution for ζ implied by our results. Our results suggest 90% and 95% confidence limits of $\zeta > -0.09$ and $\zeta > -0.3$ respectively.

Subject headings: accretion, accretion disks – black holes – galaxies:nuclei – X-rays:spectra

1. Introduction

Black holes (BHs) are among the simplest objects in nature, able to be defined completely by mass and spin alone. But whereas the mass of a BH is relatively easy to calculate, provided material orbiting the BH can be observed, spin has proven much more challenging to constrain. The advent of high-resolution X-ray spectroscopy and the promising development of gravitational

[1]NASA's GSFC, mail code 662, Greenbelt MD 20771

[2]Dept. of Astronomy, University of Maryland, College Park, College Park MD 20742

wave detectors are now making this field of research accessible. This paper represents the first-ever survey to quantify the angular momenta of BHs in a sample of AGN using relativistically broadened iron lines as spin diagnostics. We anticipate that this work will serve as a stepping stone for guiding future spin surveys across a wide range of environments, including AGN of varying host galaxy morphology, and supermassive BHs vs. stellar-mass BHs, to name two interesting population comparisons.

A General Relativistic effect, BH spin manifests itself physically by setting the radius of the effective inner edge of the accretion disk: as the magnitude of the (prograde) spin increases, frame-dragging provides matter in the disk with additional angular momentum with which to resist the inward pull of gravity, enabling this material to remain in orbit nearer to the event horizon than it would in such close proximity to a non-spinning BH. The inner edge of the disk can therefore be used to measure BH spin (Reynolds & Fabian 2008).

The position of the inner edge of the accretion disk can be constrained through detailed modeling of the X-ray spectrum of the disk. Two popular modeling schemes include fitting the thermal continuum of the disk (Narayan et al. 2007) and fitting the shape of the fluorescent Fe-K line emitted by the disk in response to irradiation by the X-ray power-law (Brenneman & Reynolds 2006). The former method relies on *a priori* knowledge of the BH mass and distance as well as the disk inclination angle, however, and is also only applicable to smaller Galactic BH systems (GBHs) in thermally dominant states as opposed to supermassive BHs found in the centers of active galactic nuclei (AGN). By constrast, the shape of the iron line profile depends upon the gravitational redshift and fluid velocity field, both of which depend only upon M/R. The iron line profile is therefore mass-independent, making it a useful technique for any BH system (Reynolds & Nowak 2003), but especially for AGN in which the NH mass is often poorly determined.

The shape of the iron line profile is determined by several physical parameters: the BH angular momentum, the radial extent of the disk, the emissivity profile of the disk, the inclination angle of the disk to the observer's line of sight and the flux in the line itself as compared to the continuum flux. A proper model for the iron line must also take into account the effects of the Doppler shift, Special Relativity (e.g., beaming) and General Relativity (e.g., gravitational redshift). Unfortunately, the two widely available models within the XSPEC spectral analysis software for these types of fluorescent disk lines emitted near a BH do not take all of these physical effects and parameters into account. BH spin, in particular, is not a free parameter in either the `diskline` model for non-spinning Schwarzschild BHs (Fabian 1989) or the `laor` model for maximally-rotating Kerr BHs (Laor 1991). Both of these codes have their dimensionless BH spins hardwired at $a = 0$ and $a = 0.998$, respectively, where $a \equiv cJ/GM^2$. If one wishes to constrain BH spin, therefore, it is necessary to create a new, fully-relativistic model code which enables the BH spin to be fit as a free parameter.

We have developed such a model as both a line code (`kerrdisk`) and a convolution kernel (`kerrconv`) that can be applied to a full spectrum of fluorescent emission lines from the disk. These models were introduced and detailed in Brenneman & Reynolds (2006), hereafter known as BR06. In that paper we also presented a series of model fits to the 330 ks *XMM-Newton*/EPIC-pn spectrum of the canonical broad iron line Sy-1 AGN MCG–6-30-15, noting that the best fit was achieved with a `kerrconv` model acting on an ionized disk reflection spectrum, where the inner edge of the disk was $r_{\rm min} \leq 1.62 r_{\rm g}$. These data have allowed us to place formal constraints on the BH spin in MCG–6-30-15 of $a > 0.987$ (90% confidence level). Because this fit was performed under the assumption of a strict truncation of the iron line region at the innermost stable circular orbit (ISCO) in the disk, this constraint is somewhat weakened ($a > 0.94$) if the iron line emission region does in fact bleed inside of the ISCO (Reynolds & Fabian 2008). Given that MGC–6-30-15 harbors the broadest iron line in an AGN observed to date, this model fit reinforces our expectation that this AGN contains a BH of near-maximal spin. Many other, similar Sy-1 galaxies are also observed to have broad iron lines, however (Guainazzi et al. 2006; Nandra et al. 2007; Miller 2007), which begs two important questions: (1) can *XMM-Newton* observations of broad iron lines be used to robustly constrain BH spin, and (2) how is spin distributed between and among different types of BH systems?

To begin addressing these questions, we have collected a sample of eight other Sy-1 AGN from the *XMM-Newton* archive that have previously been observed to have broad iron lines. Using the same technique we used to model the spectrum of MCG–6-30-15 by first addressing the continuum and absorption and then considering the broad line region, we assess each AGN independently, with the goal of obtaining statistically robust BH spin constraints whenever possible.

The question of what BH spin distribution we should expect to see among Sy-1 AGN is not a simple one. Unlike GBHs, whose spins are thought to be chiefly natal due to the small masses and/or short lifetimes of their stellar companions, AGN are old and massive, and are thought to have grown from a combination of mergers and accretion over their long histories. By comparing observations of BHs in local galaxies and AGN to a model of what the BH mass function would look like for a given local population whose BHs were grown solely by accretion, Marconi et al. (2004) find that mergers are not significant in the evolution of local supermassive BHs. The authors suggest that mergers might play a more prominent role for SMBHs beyond $z = 3$. Determining the spin of such sources would therefore provide us with a new parameter to use in constraining the role and efficiency of accretion in evolving local SMBHs, and would also aid in assessing the relative contributions of accretion vs. mergers in higher redshift sources. Similarly, Volonteri et al. (2005) have used numerical simulations to predict how massive BHs should form and evolve. They find that the coalescence of comparable-mass BHs increases their BH spins, while the capture of smaller BH companions in randomly oriented orbits reduces the spin of the primary BH. Given the distribution of massive BH binary mass ratios in hierarchical models, binary

mergers alone do not lead to a systematic spin-up or spin-down of SMBHs with time. By contrast, because of the alignment of a SMBH with the angular momentum of the outer accretion disk, gas accretion tends to increase BH spin over time. Overall in the Volonteri et al. models, accretion dominates over mergers and efficiently increases BH spin. The spin distribution is heavily skewed toward rapidly rotating holes, is already in place at early epochs, and does not change much below $z = 5$. If accretion occurs via a geometrically thin disk, about 70% of all massive BHs are close to maximally rotating. Even in the conservative case in which accretion is via a geometrically thick disk, about 80% of all massive BHs have $a > 0.8$ (Volonteri et al. 2005). King, Pringle & Hofmann (2008), however, use simulations to contend that black hole growth in AGN proceeds by accretion from random directions such that the average BH spin ranges from $a = 0.1 - 0.3$, with mergers making little difference. These authors argue that more massive BHs would tend to have smaller spins, and that the "rare" examples of massive BHs with large spins would likely result from prograde mergers of SMBHs with similar masses and would therefore be most often found in giant elliptical host galaxies (King et al. 2008). Given these disparate theoretical predictions and the increasing computing power of complex numerical simulations, the time is ripe for culling observational evidence to investigate whether the data support such hypotheses.

In order to begin probing the question of BH spin distribution across the AGN population we clearly need to expand our sample. In this paper we restrict our attention to several other nearby Sy-1 AGN in an effort to reduce the number of environmental variables that may be involved in spin determination (e.g., no GBHs, though we do intend to expand our source list further in the future to accommodate such objects and compare the results to those of our AGN sample). Because the `kerrdisk` and `kerrconv` models rely on the presence of broad iron lines in the X-ray spectrum in order to constrain BH spin, we have also restricted our source list to include only those Sy-1 AGN that have robustly been observed to harbor broad iron lines based on previous studies with *XMM-Newton* and/or *Chandra* (Nandra et al. 2007; Miller 2007).

Section 2 discusses the observations of the sources in our sample and the method used to reduce the EPIC-pn data and extract spectra. A summary of our modeling technique is given in §3. Results and tables comparing the relevant best-fit parameters for each source can be found in §4. Implications of these results, conclusions we have drawn and a prognosis for future work in this field are discussed in §5. The Appendix contains the detailed spectral fitting results for each source.

2. Observations and Data Reduction

Our source selection was based on recent work by Nandra et al. (2007) and the review by Miller (2007), both of whom consider the robustness of broad iron line detections across different

source populations. The Miller review, in particular, collects all the recent X-ray data published on Seyfert sources and categorizes these objects by the strength and robustness of their broad iron line features. We have used these two studies as a guide for selecting the candidates for our sample.

Our data have been collected from the *XMM-Newton* Science Archive, using only publicly available observations. *XMM-Newton* data were preferentially used as opposed to *Chandra* data because of the superior collecting area of *XMM-Newton* in the $2-10\,\mathrm{keV}$ band where the broad Fe-Kα feature is the most prominent. Though *Suzaku* is producing very interesting results, there are not enough publicly available data collected by that instrument to undertake such a study at this time.

We focus our study exclusively on the EPIC-pn data to avoid cross-calibration issues between the pn, MOS and RGS instruments. Though the RGS spectra in particular can provide detailed insight into the $0.3-2.0\,\mathrm{keV}$ spectrum and help illuminate the nature of the soft absorption and excess seen in so many Sy-1 AGN, the cross-calibration issues unfortunately render it nearly impossible to correlate those results with the continuum and iron line spectrum observed by the EPIC-pn instrument. For further discussion of this issue, see Brenneman et al. (2007) and references therein. Because of the higher effective area of the pn, these data are more useful in our work. Observation data for each source is shown in Table 1.

For each source in question we performed reprocessing (when necessary) and data reduction with the SAS version 7.0.0 software, including the latest CCF calibration files. We have used the SAS `epatplot` task to compute the fraction of single, double, triple and quadruple events as a function of energy and compared these fractions to their nominal values as measured from weak source observations. For sources that are affected by pile up, these fractions deviate from the nominal values due to the higher probability of wrong pattern classification. No significant deviation from the nominal single and double distributions was found for any of our sources, indicating that our EPIC-pn observations are not affected by pile up. Source and background spectra and light curves were extracted using the `xmmselect` task from the SAS GUI. Response matrices and ancillary response files were generated using the `rmfgen` and `arfgen` tasks. These were then grouped with the spectral files using the FTOOLS package `grppha` with a minimum of 25 counts/bin in order to use χ^2 as a meaningful goodness-of-fit statistic. Spectral analysis was carried out as before for MCG–6-30-15 (BR06) with XSPEC version 11.3.2 and our local `kerrdisk` and `kerrconv` models installed.[1]

[1]These models are available for download and use in XSPEC from http://www.astro.umd.edu/ chris/publications/papers/kerrdisk/kerrdisk_model.html.

AGN	Date Obs.	Exposure (s)	Counts	pn Mode	Filter	RA (h)	Dec. (°)	z	Source Type
MCG–6-30-15	7/31/2001	331330	6.5×10^6	PSW	Medium	13.5983	−34.2958	0.0077	Sy-1.2
MCG–5-23-16	12/8/2005	121578	2.2×10^6	LW	Medium	9.7945	−30.7489	0.0085	Sy-1.9
Mrk 766	5/20/2001	111789	2.9×10^6	PSW	Medium	12.3074	29.8128	0.0129	Sy-1.5, NLS1
NGC 3783	12/19/2001	131025	1.8×10^6	PSW	Medium	11.6505	−37.7385	0.0097	Sy-1
NGC 4051	5/16/2001	121889	3.3×10^6	PSW	Medium	12.0527	44.5313	0.0023	Sy-1.5, NLS1
Fairall 9	7/5/2000	29209	4.0×10^5	PFW	Medium	1.3961	−58.8058	0.0470	Sy-1
Ark 120	8/24/2003	112130	2.7×10^6	PSW	Thin1	5.2699	−0.1502	0.0327	Sy-1
NGC 2992	5/19/2003	28917	6.0×10^5	PFW	Medium	9.7617	−14.3264	0.0077	Sy-1.9
3c273	6/30/2004	19861	7.5×10^5	PSW	Thin1	12.4852	2.0524	0.1583	QSO, Sy-1

Table 1: Observation parameters for the eight AGN in our sample of broad iron line sources, plus the long observation of MCG–6-30-15 (Fabian et al. 2002) discussed at length in BR06.

3. Spectral Analysis Methodology

In the following Section we outline the method used for the data reduction and spectral analysis of the AGN in our sample. We then compare the results from all the sources in our sample and discuss their physical implications for BH spin distribution and evolution among Sy-1 AGN. For spectral modeling and results from the individual sources in our sample, see the Appendix.

3.1. Continuum Fitting

We have endeavored to make the spectral analysis method as uniform as possible for all the AGN examined. There are, however, certain intrinsic physical differences between the sources that must be taken into account in order to properly model the continuum and isolate the iron line(s) in each case. Though all of our sources are Sy-1 AGN (or otherwise observed in states where they manifest broad disk lines), each system is unique in its physical properties. Some have more photons than others to work with, either because of higher flux, longer observation time or both. Some exhibit evidence for complex, multi-zone warm absorbers (WAs) intrinsic to the central engine, whereas some show only cold absorption from neutral hydrogen along our line of sight. A soft excess is seen in some sources but not others. And of course, the strength and breadth of the Fe-Kα line varies from source to source as well, though all have been chosen because they have previously shown evidence for broad iron lines.

In order to examine the iron line(s) in detail the continuum must first be accurately modeled. After excluding the energy ranges relevant to the iron line ($\sim 4.0 - 8.0\,\mathrm{keV}$) and the mirror edges ($\sim 1.5 - 2.5\,\mathrm{keV}$), we examine the rest of the $0.6 - 10.0\,\mathrm{keV}$ spectrum, fitting it with a power-law continuum typical of an AGN which is then modified by cold photoabsorption from neutral hydrogen. We set the minimum value of N_{H} equal to the Galactic column density along our line of sight to the source[2] and allow it to vary as necessary to accommodate the cold absorption in the system. Some sources require a second, unabsorbed power-law component as well to properly model the basic continuum shape. We disregard energies below $\sim 0.6\,\mathrm{keV}$ due to calibration uncertainties in this range for the EPIC-pn instrument.

If significant residual features remain after fitting this absorbed power-law which indicate the presence of a soft excess and/or warm absorption, we include these components one by one as long as they make a significant difference in the global goodness-of-fit according to the F-test ($\Delta\chi^2 \leq -4$ for each new parameter introduced into the fit (Bevington 1969)). The soft excess is

[2]This parameter is determined from H I 21 cm surveys. See http://heasarc.gsfc.nasa.gov/cgi-bin/Tools/w3nh/w3nh.pl for the column density calculator as well as Dickey & Lockman (1990).

typically parameterized by a blackbody component representing thermal emission in the central engine, but may also be modeled by bremsstrahlung emission or Comptonized emission from a thermal disk if either of these more complex forms gives a significantly better reduction in χ^2. The warm absorption is modeled using the same XSTAR-generated multiplicative table model described in Brenneman et al. (2007) and BR06 in the analyses of NGC 4593 and MCG–6-30-15. Solar abundances are assumed for all elements and the redshift is set at the source value. Some AGN show no need for a WA model, while others statistically require up to two physically separate WA components, each exhibiting a distinct column density ($N_{\rm H}$) and ionization parameter (ξ).

Once the continuum has been properly modeled, we freeze the parameter values for all components except the power-law spectral index (Γ) and normalization (flux in $\rm ph\,cm^{-2}\,s^{-1}$) and restrict our energy range from $2.5-10.0\,$keV in order to focus on the hard X-ray spectrum and the iron line region. Including the energies from $4.0-8.0\,$keV again, we check for residual emission (or absorption) lines from $6.4-6.97\,$keV, indicating the presence of unmodeled neutral and/or partly ionized Fe-Kα in the spectrum. Because these sources have been pre-determined to possess significant, broadened iron emission, such residual emission features are seen in each case. We begin by attempting to fit the $6.4\,$keV line of neutral iron (and any other ionized lines) with a simple Gaussian feature, with the line width frozen at $\sigma = 0\,$keV (i.e., intrinsically narrow) and the redshift again set to the source value. As expected, in each case we note significant residual "wings" remaining around the Fe-Kα feature after this narrow core was fit, indicating the presence of a broad component to the line.

3.2. Fitting the Iron Line Profile

To assess the robustness of the broad iron component and to obtain constraints on the BH spin, if possible, we follow our continuum fitting procedure (including modeling the narrow core of the iron line) by running each source through an "analysis tree" of progressively more complex modeling in the broad iron line region. Our procedure is outlined below:

1. We begin by adding in a broad iron line described by the `laor` model (spin hardwired at $a = 0.998$) at the energy of the cold Fe-Kα line and refit, noting the corresponding change in $\chi^2/{\rm dof}$ to verify whether a broad line is statistically warranted in the model. We also note the inner radius of disk emission: a broad line with the potential to diagnose BH spin should have an inner disk radius of $r_{\rm min} \lesssim 6\,r_{\rm g}$. We relax this restriction here to allow for differences in fit that may be achieved through different models, requiring that $r_{\rm min} \lesssim 20\,r_{\rm g}$.

    - If the broad line is *not* statistically warranted, we simply constrain the upper limit of the equivalent width of the line.

- If the broad line is at least marginally statistically warranted, we replace the `laor` component with a `kerrdisk` component ($a = 0 - 0.998$) and refit, noting again the corresponding change in χ^2/dof. The inner disk radius and BH spin as well as their statistical constraints should also be noted.

2. Rather than simply modeling the Fe-Kα line in isolation, we replace the broad line component with a static ionized disk reflection spectrum (Ross & Fabian 2005) and fit.

3. Starting from the static ionized disk reflection sprctrum, we add in the effects of relativistic smearing from the spacetime around a maximally rotating BH using the `kdblur` convolution model ($a = 0.998$). Again we note the statistical difference in the goodness-of-fit to determine the importance of relativistic effects (our criterion again being F-test statistics), as well as the inner radius of disk emission. This procedure gives us a rigorous measure of the degree to which broadening is required even when reflection is accounted for.

   - If the inner radius of disk emission is sufficiently close to the event horizon (again using $r_{\rm min} \lesssim 20 r_{\rm g}$), the line may be sufficiently broad and relativistic effects may be sufficiently important to allow us to constrain BH spin. In this case, we replace the `kdblur` component with `kerrconv` ($a = 0 - 0.998$) in order to obtain statistical constraints on $r_{\rm min}$ and a.

We force the outer radius of disk emission to be $r_{\rm max} = 400 r_{\rm g}$ (or $400 r_{\rm ms}$ in the case of `kerrdisk` and `kerrconv`, which parameterize disk emission radius in units of the radius of marginal stability) in all the broad line fits. The value itself is somewhat arbitrary; as long as $\alpha > 2$ emission from this part of the disk is negligible. For the ionized disk component, we begin with the assumption of solar iron abundance and relative neutrality (Fe/solar $= 1$ and $\xi = 30\,{\rm erg\,cm^{-1}\,s^{-1}}$). We then relax these assumptions and allow these two parameters to fit freely, provided that reasonable statistical error bars can still be obtained for each parameter. For `kerrdisk` and `kerrconv`, we initially assume that the inner and outer portions of the disk emit under the same emissivity index: $\alpha_1 = \alpha_2$, where the disk radiates as $r^{-\alpha}$ at any given radius. Again, if the fit is sufficiently robust, these indices are "untied" and allowed to each fit freely, but due to limitations in the number of photons we have for each data set, the only source with enough counts to support a scenario where $\alpha_1 \neq \alpha_2$ is MCG–6-30-15.

4. Sample Results

We have compiled the relevant parameter constraints from all of our spectral fits to nine Sy-1 sources: MCG–6-30-15, MCG–5-23-16, Mrk 766, NGC 3783, NGC 4051, Ark 120, Fairall 9,

NGC 2992, and 3c273. The constraints on the relativistic disk parameters for each object are presented in Tables 2-4. Note that in each case a model including reflection from an ionized disk convolved with a relativistic smearing kernel provides the best statistical fit, and that in almost every case the `kerrconv` model (with arbitrary spin) provides a better fit than the `kdblur` model (spin fixed at $a = 0.998$).

Previous studies have indicated that broad iron lines may be present in up to 42% of AGN observed with the *XMM-Newton*/EPIC-pn camera that have $\gtrsim 10^4$ counts (Guainazzi et al. 2006). To assess whether evidence exists for a relativistically broadened iron line in each of our data sets, we first considered the `laor` fits in which BH spin is fixed at $a = 0.998$. While each source demonstrated a significant improvement in its global fit as compared to a model fitting only a narrow iron line core with a Gaussian component, the important parameter to evaluate in this case is the inner radius of disk emission. Roughly speaking, as stated in §3.2, if $r_{\rm min} \lesssim 20\,r_{\rm g}$ we can say with some confidence that there is substantial emission from the inner part of the accretion disk where relativistic effects (such as BH spin) become important in shaping the overall iron line profile. Out of our nine sources, four did *not* meet this criterion outright (MCG–5-23-16, NGC 3783, Ark 120, and Fairall 9). Allowing for arbitrary BH spin via `kerrdisk` instead of `laor` does help the situation somewhat: only NGC 3783 did not meet the $r_{\rm min}$ criterion in this fit, though for none of the sources is the global fit greatly improved over its `laor` value. Fairall 9 and 3c273 have spins that cannot be constrained with the `kerrdisk` model. The `laor` and `kerrdisk` fits are presented in Table 2.

We have also examined the question of how robust the presence of a broad line is in the spectrum when reflection is included. Beginning with a base continuum model including a static ionized disk reflection spectrum (Ross & Fabian 2005), we noted the overall goodness-of-fit and the residual features remaining, especially around the iron line region. We then convolved this model with relativistic effects, first using the `kdblur` smearing kernel (Table 3), then substituting in `kerrconv` (Table 4). A significant improvement in the global fit with `kdblur` indicates that relativistic smearing is important in the system, and further significant improvement with `kerrconv` instead of `kdblur` indicates that although relativity is important, in the best fit scenario the BH spin deviates from its maximal value. Whenever possible we allowed the iron abundance and ionization parameter to fit freely in the ionized disk model, though in some cases these additional degrees of freedom prevented us from obtaining a reliable fit. For these sources it was necessary to assume a neutral disk ($\xi = 30\,{\rm erg\,cm^{-1}\,s^{-1}}$) and solar iron abundance (Fe/solar=1): Ark 120, Fairall 9 and 3c273. The `kdblur` and `kerrconv` fits returned similar results in terms of parameter constraints and overall fit to the iron line profile in each source, and in nearly all cases also produced a statistically significant improvement in the overall goodness-of-fit, with the exception being NGC 3783, in which only a marginal improvement in the goodness-of-fit was seen. These results demonstrate that relativistic smearing is strongly required in nearly all of our sources, even after static reflection

is included.

The `reflion` model does not include a formal parameter for the reflection fraction of the disk, so in order to facilitate comparison between our results and those from studies using other models to parameterize reflection (e.g., `pexrav`), we have estimated $R_{\rm refl}$ in our best-fit model (`kerrconv(refl)`). To perform this calculation, we have assumed that for $R_{\rm refl} = 1$, half of the radiation from the hard X-ray power-law is received and reflected by the disk, with the other half traveling directly to the observer. Reflection fractions of greater than unity then indicate that more than half of the power-law radiation illuminates the disk, implying anisotropic emission from the power-law source or perhaps strong light-bending of this emission near the BH. $R_{\rm refl} < 1$ means that some of the power-law emission is either absorbed or scattered away before reaching the disk. We compute $R_{\rm refl}$ using the following formula:

$$R_{\rm refl} = \frac{N_{\rm refl}}{N_{\rm po}} \frac{F_{\rm refl}}{F_{\rm po}} \left(\frac{\xi}{30}\right)^{-1} \quad (1)$$

Here $N_{\rm refl}$ and $N_{\rm po}$ denote the normalizations of the `reflion` and power-law components from the best-fit model from $2.5-10.0\,$keV, $(\xi/30)$ is the best-fit ionization parameter with respect to "neutral" in the `reflion` component, and $F_{\rm refl}$ and $F_{\rm po}$ are the fluxes contained in the `reflion` and power-law components for unity normalization over the full wavelength range ($0.001-1000\,$keV). The estimated reflection fraction for the best-fit model, $R_{\rm refl}$, including errors, is shown in Table 4.

We have obtained formal constraints on BH spin in four of the eight new cases: Ark 120 ($a = 0.63-0.68$), Mrk 766 ($a > 0.85$), NGC 4051 ($a > 0.67$) and 3c273 ($a > 0.72$). In comparison, the best fit to MCG–6-30-15 yields $a > 0.96$ from $2.5-10.0\,$keV and $a > 0.987$ based on our $0.6-10.0\,$keV fit discussed in BR06. The two MCG–6 results differ slightly due to the different energy ranges modeled in BR06 vs. this paper. We were unable to constrain BH spin in MCG–5-23-16, NGC 3783, Fairall 9 and NGC 2992 in the `kerrconv` fits.

There are several potential reasons why one might not be able to obtain a good spin constraint for a given source. Firstly, a lack of sufficient photons in the data set is a severe limitation for obvious reasons. This is certainly the case in 3c273, for example, and also plays a role in the spectra of NGC 2992 and Fairall 9. Generally speaking, the more photons one has to work with, the better the fit constraints will be.

Secondly, if the iron line is not sufficiently broad, the relativistic parameters will be more difficult to constrain. A narrow iron line could originate from far out in the disk, away from the spacetime where relativistic effects become imprinted on the line profile. This scenario would leave us with no way to know the spin of the BH. Even iron lines from the inner regions of disks around non-spinning BHs show the spectral signatures of relativity, as shown in BR06, so if the line originates reasonably close to a non-spinning BH, we should be able to constrain its spin.

Therefore, we should not be surprised that the sources for which we are unable to get spin constraints all share a common characteristic: constraints on $r_{\rm min}$ that fall outside the inner portion of the disk, i.e., well outside of $6r_{\rm g}$.

Our methodology uses the degree of relativistic smearing (and principally the broadening of the iron line) to constrain black hole spin *on the assumption that the inner radius of the iron line emitting region cannot be smaller than the ISCO*. Even allowing for some emission to originate within the ISCO will not significantly alter the iron line profile (Reynolds & Fabian 2008). However, one can readily envisage scenarios whereby the iron line emission can truncate at radii larger than the ISCO, for example, due to a very highly ionized inner disk or a transition to a radiatively-inefficient accretion flow. This leads to an important (approximate) degeneracy in our model fits; since our spin constraints are primarily driven by modeling the maximum redshift of the iron line (rather than higher order details of line profile), the possibility that the line emitting region can truncate outside of the ISCO implies that our derived spin constraints will be in the form of lower limits. This is indeed what we find in three out of our four cases (excluding MCG–6-30-15). In the case of Ark 120, the accretion disk appears to be rather edge-on and (within the context of our spectral model) strong light bending effects around this highly inclined disk allow the degeneracy between a and $r_{\rm min}$ to be broken. However, for more face-on disks, exceptional signal-to-noise data (exceeding that possible from *XMM-Newton*) is required to break this degeneracy via details of the line profile.

AGN	α	a	$i(^\circ)$	$r_{\rm min}\,(r_{\rm g})$	χ^2/dof
MCG–6-30-15	$2.84-2.95$	0.998	$30-32$	$1.71-2.11$	940/1002 (0.94)
	$5.93-6.37, 2.27-2.46, 10.28-13.99$	$0.97-0.98$	$30-31$	$1.68-2.67$	907/999 (0.91)
MCG–5-23-16	$1.98-4.30$	0.998	$21-37$	$18-44$	1509/1490 (1.01)
	$2.27-2.82$	<0.71	$38-39$	$32-65$	1514/1489 (1.03)
Mrk 766	$1.78-2.05$	0.998	$85-86$	$1.24-1.82$	1542/1311 (1.18)
	$2.14-2.33$	$0.39-0.62$	$77-78$	$4.41-4.67$	1539/1310 (1.17)
NGC 3783	$9.23-10.00$	0.998	<18	$1.24-1.80$	1741/1489 (1.17)
	$---$	>0.89	$17-18$	$315-388$	1732/1488 (1.16)
NGC 4051	$2.45-3.63$	0.998	$30-39$	$3.96-6.98$	1480/1397 (1.06)
	$4.24-10.00$	<0.87	$32-41$	$3.63-5.67$	1479/1396 (1.06)
Fairall 9	$1.40-2.70$	0.998	>50	$1.24-25$	672/692 (0.97)
	$1.79-3.50$	$---$	$52-69$	$3.86-59$	671/691 (0.97)
Ark 120	$---$	0.998	$52-69$	>150.00	1639/1422 (1.15)
	$1.65-1.98$	<0.69	$67-69$	$3.94-6.43$	1620/1421 (1.14)
NGC 2992	$1.31-3.15$	0.998	$37-55$	$3.07-4.27$	1399/1310 (1.07)
	$3.90-10.00$	>0.97	$38-49$	$1.67-6.22$	1399/1309 (1.07)
3c273	$2.83-6.37$	0.998	<67	$1.24-3.18$	228/267 (0.854)
	$---$	$---$	<35	$1.64-3.99$	229/266 (0.86)

Table 2: Comparison of the spectral fitting results for the $2.5-10.0$ keV spectra using the `laor` and `kerrdisk` models. All AGN in our sample that are thought to possess broad iron lines are presented, as well as the MCG–6-30-15 data from BR06 re-fitted with these models from $2.5-10$ keV, in keeping with our current sample. For each source the top row represents the `laor` range in parameter value while the bottom row represents the `kerrdisk` range in parameter value. Ranges are given at 90% confidence. Note that MCG–6-30-15 is able to be fit with a broken power-law emissivity index, which is listed under α as α_1, α_2, $r_{\rm br}\,(r_{\rm g})$. For all other sources, $\alpha_1 = \alpha_2$ and $r_{\rm br} = 6.0\,r_{\rm g}$.

AGN	Fe/solar	$\xi_{\rm refl}$ (erg cm^{-1} s^{-1})	α	i (°)	$r_{\rm min}$ ($r_{\rm g}$)	χ^2/dof
MCG–6-30-15	9.57 – 10.00	249 – 273				1296/1003 (1.29)
	5.97 – 10.00	< 39	8.89 – 10.00	39 – 40	4.47 – 4.94	887/1000 (0.87)
MCG–5-23-16	0.53 – 0.83	< 34				1555/1492 (1.04)
	0.48 – 0.72	< 31	1.05 – 4.40	22 – 37	1.24 – 64	1485/1488 (1.00)
Mrk 766	1.00	1742 – 3886				1534/1313 (1.17)
	1.00	413 – 672	1.71 – 2.04	73 – 81	1.24 – 2.96	1495/1310 (1.14)
NGC 3783	0.18 – 0.34	< 53				1534/1490 (1.03)
	0.14 – 0.23	< 46	– – –	< 35	> 102	1525/1487 (1.03)
NGC 4051	1.21 – 4.27	< 57				1506/1398 (1.08)
	1.29 – 10.00	< 122	3.08 – 4.29	32 – 38	1.24 – 7.36	1476/1395 (1.06)
Fairall 9	1.00	30.00				680/695 (0.98)
	1.00	30.00	2.47 – 10.00	50 – 87	1.24 – 8.25	665/692 (0.96)
Ark 120	1.00	30.00				1717/1425 (1.20)
	1.00	30.00	1.59 – 1.83	82 – 86	1.24 – 2.02	1576/1422 (1.11)
NGC 2992	1.00	30.00				1414/1313 (1.08)
	1.00	30.00	1.50 – 4.17	17 – 42	– – –	1405/1310 (1.07)
3c273	1.00	30.00				235/269 (0.87)
	1.00	30.00	2.45 – 10.00	< 60	1.24 – 11	228/266 (0.86)

Table 3: Comparison of the spectral fitting results for the 2.5 – 10.0 keV spectra using the ionized reflection model `reflion` and `kdblur(refl)`, which convolves the reflection spectrum with a smearing kernel from a maximally-spinning BH. For each column of data, the top row represents the `reflion` range in parameter values while the bottom row represents the `kdblur(refl)` range in parameter values. For the `reflion` component, the value of the incident power-law spectral index is set equal to that of the continuum. Ranges are given at 90% confidence.

AGN	Fe/solar	$\xi_{\rm refl}$ (erg cm^{-1} s^{-1})	$R_{\rm refl}$	α	a	i(°)	$r_{\rm min}$ ($r_{\rm g}$)	χ^2/dof
MCG–6-30-15	4.75 – 10.00	< 83	1.03 – 1.57	5.46 – 6.95, 2.34 – 2.66, 7 – 11	> 0.96	30 – 32	1.43 – 2.22	834/997 (0.84)
MCG–5-23-16	0.55 – 0.69	< 31	0.39 – 0.43	1.84 – 3.04	– – –	26 – 48	44 – 152	1483/1487 (1.00)
Mrk 766	1.00	444 – 852	2.22 – 2.86	1.80 – 2.08	> 0.85	73 – 81	< 2.78	1492/1309 (1.14)
NGC 3783	0.15 – 0.22	< 40	1.13 – 1.91	– – –	– – –	26 – 46	< 983	1526/1486 (1.03)
NGC 4051	1.25 – 5.69	< 108	0.28 – 2.00	4.23 – 10.00	> 0.67	36 – 40	3.50 – 7.19	1475/1394 (1.06)
Fairall 9	1.00	30.00	1.76 – 4.00	1.86 – 10.00	– – –	52 – 64	– – –	665/691 (0.96)
Ark 120	1.00	30.00	2.12 – 3.23	2.29 – 2.44	0.63 – 0.68	79 – 80	3.62 – 3.95	1543/1421 (1.09)
NGC 2992	1.00	30.00	0.44 – 0.86	1.24 – 10.00	– – –	20 – 48	5.57 – 12.00	1402/1312 (1.07)
3c273	1.00	< 356	0.92 – 33.10	2.74 – 10.00	> 0.72	< 63	1.24 – 2.84	228/265 (0.86)

Table 4: Comparison of the spectral fitting results for the 2.5 – 10.0 keV spectra using the ionized reflection model `reflion` convolved with a smearing kernel from a BH of arbitrary spin `kerrconv`. All AGN in our sample are presented, as well as MCG–6-30-15, based on the fits shown above in Tables 2-3. For the `reflion` component, the value of the incident power-law spectral index is set equal to that of the continuum. Parameter value ranges are given at 90% confidence. Note that MCG–6-30-15 is able to be fit with a broken power-law emissivity index, which is listed under α as α_1, α_2, $r_{\rm br}$ ($r_{\rm g}$). For all other sources, $\alpha_1 = \alpha_2$ and $r_{\rm br} = 6.0\,r_{\rm g}$. Reflection fraction is estimated as described above in the text, based on the relative fluxes and normalizations of the power-law and `reflion` components of this best-fit model.

5. Discussion and Conclusions

This paper explores the use of broad iron emission lines to constrain black hole spin, and makes the first steps toward estimating the spins in a small and relatively homogeneous sample of AGN. Following our previous work on MCG–6-30-15 (BR06), this study of an additional eight prominent Sy-1 AGN observed to have prominent iron lines has provided us with some intriguing data on this subject and has also put us in an excellent position to apply our spectral fitting techniques to many other sources in the future.

5.1. Implications of our Sample Results

Though our total sample of nine Sy-1 AGN is far too small to allow us to draw any robust conclusions about the distribution of BH spins in this group of objects as a whole, this work has allowed us to design a viable method for evaluating the presence of a broad iron line in the data and using it to place constraints on the BH spin with our new models, `kerrdisk` and `kerrconv`. Based on our data analysis we have arrived at several important conclusions that we hope will inform subsequent BH spin surveys:

1. Guainazzi et al. (2006) found that the number of broad iron lines observed in AGN increases dramatically when the data have more than $\sim 10^4$ counts. Similarly, we find that it is necessary to have a certain minimum number of photons in order to have a spectrum of the quality needed to extract spin information. Based on our results, this number appears to be on the order of $\sim 10^6$ photons. This makes sense, given that spectral line fitting of any kind is a statistical process and without enough data points one cannot expect to model a line with any statistical certainty.

2. A broad iron line is needed in order to constrain spin. Simply put, a narrow line cannot represent emission from the inner part of the disk; if it were, it would show signatures of Doppler shifting and relativistic effects that combine to give good diagnostic disk lines such as Fe-Kα their characteristic shapes. If a line does not originate in the inner disk, then relativity is not important to its morphology, and it cannot be used as a spin diagnostic because spin is a relativistic effect.

3. Five out of nine sources from our broad Fe-K line sample (including MCG–6-30-15) showed a significant improvement in their global goodness-of-fit when relativistic smearing was added to a static ionized disk reflection spectrum.

4. Across our sample of radio-quiet Sy-1 sources, we see a mix of spin constraints from moderate to very high. We do NOT see any non-spinning sources among those with robust spin

constraints, although it is possible that those sources without good spin constraints may be slowly-spinning. **This shows that radio-loudness is not dependent on spin alone: it must be determined by at least one other parameter.** Magnetic fields and/or thick disks are likely candidates: the Blandford-Znajek process is thought to be critical in jet formation, and most sources with radio jets are hypothesized to emanate from systems with truncated thin disks (perhaps ADAFs or other types of radiatively-inefficient accretion flows).

5. Unfortunately, nature may be working against us in terms of measuring BH spin in radio-loud sources using the iron line method. Jet activity tends to overwhelm the spectrum along lines of sight to the broad line region, effectively burying the broad line and other disk signatures in many sources. Though some recent observations have noted the presence of a broad iron line in radio galaxies (e.g. 3c273, this work; 3c120, Kataoka et al. 2007), for most radio-loud AGN it may be necessary to rely on other methods of diagnosing spin.

Our five AGN with robust spin constraints all show $a > 0.3$, which seems in conflict with the theory presented by King, Pringle & Hofmann (2008) that BHs fed by accretion should tend to have spins in the range of $a = 0.1 - 0.3$ if the accretion events occur in random directions over the lifetime of the AGN. Moreover, the rapid spin seen in spiral-hosted MGC–6-30-15, in particular, also refutes the hypothesis that rapid rotators should be found in giant elliptical galaxies (King et al. 2008). Rather, our results tend to agree more with the Volonteri (2005) simulations predicting that BHs should grow mostly by accretion and evolve toward higher spins. While we are not yet able to comment on the mechanism by which our BH spins evolved, our results strongly argue against a scenario which leads to the majority of Seyfert AGN having slowly-spinning BHs. Given our limited sample size, however, more data are clearly needed in order to address these inconsistencies between theories and observations.

The last bullet point will prove to be an interesting area of research in the coming years, especially with newer, more sensitive, broader bandwidth instruments such as *Suzaku* and simultaneous X-ray/radio studies of broad line radio galaxies. The question of how BH spin correlates with radio-loudness still remains unanswered. Sikora et al. have examined the radio-loud/radio-quiet dichotomy in AGN and argue that BH spin is a critical factor in determining the radio-loudness of an AGN. The authors conclude that both spiral-hosted and elliptical-hosted AGN show radio-loudness increasing with decreasing Eddington ratio and that the large host-morphology-related difference between the radio-loudness reachable by AGN in disk vs. elliptical galaxies can be explained by the dual postulates that (1) the spin of a BH determines the jet outflow power, and (2) AGN BHs can reach large spins only in early type galaxies following major mergers (Sikora et al. 2007). The latter seems to conflict with the hypothesis that BHs most likely reach near-maximal spin values through steady accretion since mergers can theoretically occur with random BH spin directions (Volonteri et al. 2005). Also, the extremely high spin observed in MCG–6-30-15, in par-

ticular, serves as evidence that high BH spins can be found in AGN hosted by disk-type galaxies. If our 3c273 result is found to be robust, we now also have an example of a radio-loud quasar with a moderately high BH spin. These conflicts between data and theory highlight the growing need for observations of BH spin in a large sample of AGN with varying physical characteristics (e.g., mass, radio-loudness, etc.).

5.2. Formal Constraints on the Spin Distribution Function of Supermassive Black Holes

Armed with our spin constraints, we are able to observationally assess the spin distribution function (SDF) of supermassive black holes in local AGN for the first time. In doing this, we must assume that the nine sources in our sample are an unbiased subset (in terms of black hole spin) of the parent population. Since they were selected on the basis of possessing known broad iron lines, this assumption amounts to saying that the detectability of broad iron lines is unaffected by black hole spin. Significantly larger samples are required in order to actually test this assumption. However, one selection effect that might be expected results from the decreased detectability of broad iron lines due to the blending of the iron line with the continuum; this effect would be expected to bias our sample towards more slowly spinning black holes (and hence narrower iron lines).

Neglecting such selection effects, we proceed by parametrizing the SDF as a power (with index ζ) of the dimensionless spin parameter,

$$f(a) = (\zeta+1)a^{\zeta} \qquad (\zeta > -1). \tag{2}$$

We employ a Monte Carlo technique to assess the probability distribution of ζ given our data. For a given value of ζ, we conduct a trial by randomly drawing nine spins from the distribution in order to mimick the nine sources in our sample. The trial is deemed acceptable if the five spin constraints reported in Table 4 can be accommodated by the trial sample. This procedure is repeated 10^6 times for each value of ζ in a grid spanning the range $\zeta \in (-1,5)$ with spacing $\Delta\zeta = 0.01$. Assuming a uniform prior for ζ in this range, we then use the fraction of successful trials as a function of ζ to construct the probability distribution for ζ shown in Fig. 1. This distribution has a broad peak around $\zeta \sim 1$, with 90% confidence limits on ζ of $-0.01 < \zeta < 3.06$.

Being our only constraint that is *not* in the form of a lower limit, the spin measurement in Ark 120 is extremely important in setting the form of the ζ probability distribution shown in Fig. 1. Given this fact, it is interesting to examine constraints on the SDF if we exclude the Ark 120 measurement, e.g., allowing for (future) alternative explanations of the unusual Fe-K band structure in the X-ray spectrum of Ark 120. If we only have lower limits, the lack of any physical upper limit to the prior for ζ requires us to phrase our statistical question differently. Instead of constructing the

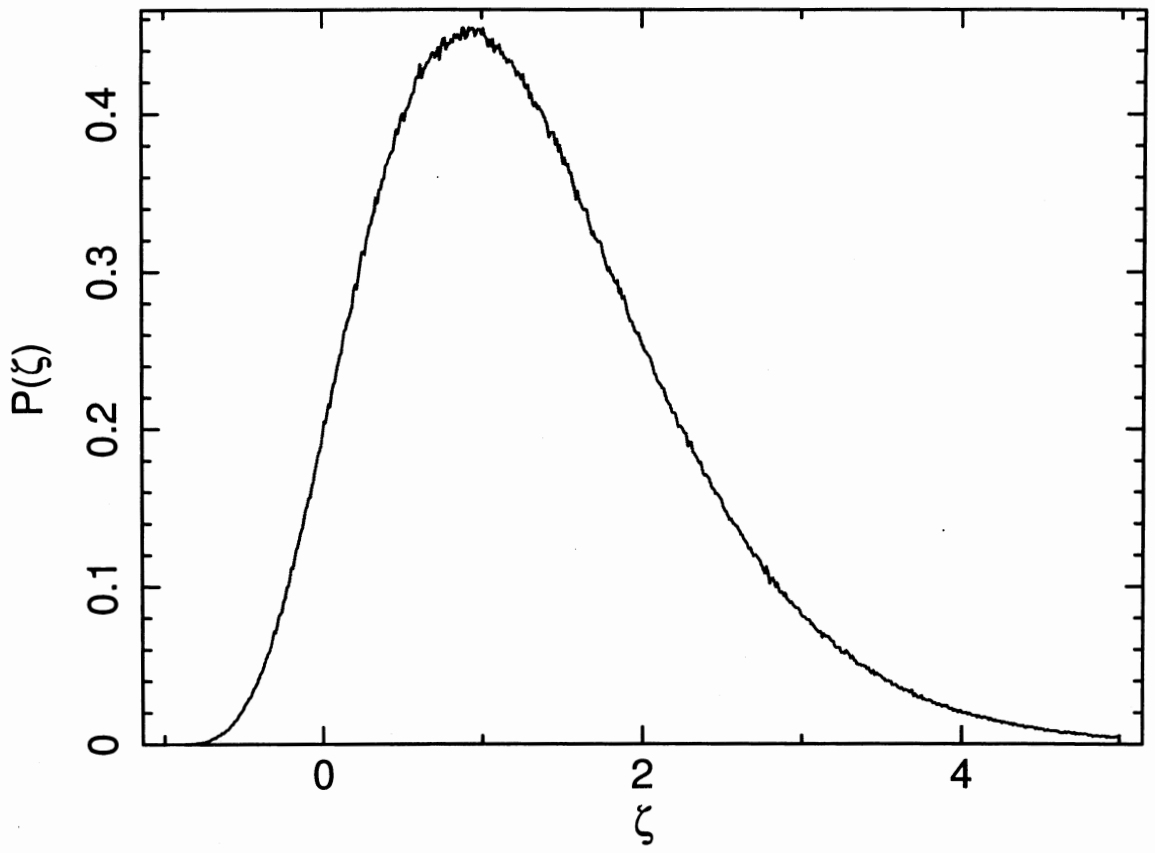

Fig. 1.— Probability distribution for the index ζ of the spin-distribution function ($f(a) = (\zeta + 1)a^{\zeta}$). See text for details and caveats of how this probability distribution is contructed.

probability distribution for ζ, we instead use our Monte Carlo technique to examine the probability P_ζ of obtaining a trial sample consistent with our observational results as a function of ζ. Given that (without Ark 120) our observational results are only in the form of lower limits, $P_\zeta \rightarrow 1$ as $\zeta \rightarrow \infty$. We find that $P_\zeta = 0.05$ when $\zeta = -0.30$ and $P_\zeta = 0.10$ when $\zeta = -0.09$. Thus, in this sense, our 90% and 95% confidence limits on ζ are $\zeta > -0.09$ and $\zeta > -0.3$, respectively.

5.3. Future Work

Because we know so little about the spin distributions of black holes, much work remains to be done in this field. While the development of free-spin models such as `kerrdisk` and `kerrconv` has allowed us to begin attacking this question quantitatively and robustly for the first time among AGN sources, our survey represents only a first step in a much larger picture. Clearly, we need more sources with broad iron lines to form a larger statistical sample. We need better quality data with more photons and higher spectral resolution in order to better constrain the BH/disk parameters in broad iron line sources. We can get this through longer observations with active observatories such as *XMM-Newton*, *Chandra* and *Suzaku*, as well as coordinated observations in other wavebands (e.g., radio and optical) which can help us form a more complete picture of the physics at work in these systems. *Suzaku*, in particular, is already proving to be an invaluable tool in the X-ray astronomer's arsenal with its ability to probe energies from $0.2 - 600\,\mathrm{keV}$. This enables the examination of the soft spectrum, iron line region and reflection peak simultaneously, greatly aiding our ability to constrain the physical parameters of the accretion disk and isolate the effect of BH spin.

We also need to expand our search radius to include stellar-mass BHs. These objects are thought to have their natal spins intact, so it will be interesting to see how the spin distribution in this population compares to that of AGN, especially given the physical similarities between AGN and GBHs in so many other areas. The advantage of the iron line method is its lack of dependence on BH mass, so this is an ideal technique to employ for such a comparison. Given the presence of other methods to diagnose BH spin, it will also be important to see how our results compare to those obtained using thermal continuum fitting, polarimetry and QPOs. Ideally, the spin constraints calculated using each different method should be consistent.

Finally, we can improve the accuracy of the `kerrdisk` and `kerrconv` models by including the effects of relativity on emission produced from within the ISCO of the disk. In so doing, however, it is crucial to properly account for the ionization level and optical depth of the material in the plunging region. Because this gas is subject to greater tidal forces and incident blueshifted radiation than the gas outside the ISCO, it is likely to be quite rarefied, optically thin and highly ionized. Proper modeling of the gas physics in this region is necessary in order to evaluate the

overall contribution of emission from this region to the broad iron line.

Acknowledgements

We gratefully acknowledge the guidance and support of the University of Maryland at College Park's Astronomy Department. Helpful contributions and advice for this work were imparted by LB's dissertation defense committee: R. Mushotzky, S. McGaugh, S. Veilleux, M. C. Miller, and T. Jacobson. We are also indebted to Andy Fabian for his insightful comments that improved this work. LB also thanks the NASA Postdoctoral Program, administered by ORAU, for her current support at NASA's GSFC. CSR gratefully acknowledges support from the National Science Foundation (grant AST 06-07428), as well as the U.Maryland/NASA-Goddard Center for Research and Exploration on Space Science and Technology (CRESST).

A. Appendix: Source-by-source Model Fitting

As mentioned in the previous Section, we have selected the AGN for our sample primarily based on the research performed by other groups on the robustness of broad iron line observations in various AGN and the likelihood of obtaining viable spin constraints from these sources using the iron line method (Nandra et al. 2007; Miller 2007). In particular, Miller (2007) discusses recent results from 30 Seyfert AGN in which relativistic disk lines have been detected and published, and divides those sources up into three "tiers" based on the nature and robustness of the detections. Many of the sources overlap with those presented in Nandra et al. Though we have examined observed spectra from all of the 9 AGN listed in Tier 1 (the most robust cases), NGC 3516 and NGC 4151 were not included in our study due to their extremely complex soft spectra (Turner et al. 2005; Schurch et al. 2004). We did analyze the other 7 sources in full: 3c120, MCG–6-30-15, MCG–5-23-16, NGC 2992, NGC 4051, NGC 3783 and Mrk 766. 3c120 is not included in this work, however, as our spectral fitting results for this object were inconclusive in several ways due to in part to a paucity of photons. We have also examined 3 other sources from Tier 3 that are mentioned prominently in Nandra et al. : Fairall 9, Ark 120 and 3c273.

We present the results of our spectral analysis for each source in its own subsection below. Note that the reflection fractions quoted are not fitted values, but rather are estimates calculated using the method described in §4 for the purpose of comparison to other studies which may model disk reflection differently (e.g., with `pexrav`). Detailed spectral fitting results for MCG–6-30-15 can be found in BR06 and are therefore not included herein.

A table of best-fit parameters for each source is included, as are figures representing the

residual broad Fe-K line feature, the best fit to the spectrum, and the best-fit model components for each object. The line residuals represent the data-to-model ratio for the best-fit model after removal of the `kerrconv(refl)` components used to fit the broad Fe-K line; the narrow line core is left in the model.

A.0.1. MCG–5-23-16

MCG–5-23-16 is a moderately absorbed Seyfert galaxy of intermediate type (Sy-1.9). It is relatively nearby at a redshift of $z = 0.0085$, and with a typical $2-10\,\mathrm{keV}$ flux of $F_{2-10} \sim 8 \times 10^{-11}\,\mathrm{erg\,cm^{-2}\,s^{-1}}$ it is one of the brightest known Seyfert galaxies (Reeves et al. 2006). The source has been observed previously to have a soft excess below $\sim 1\,\mathrm{keV}$ and an absorbing column of $N_{\mathrm{H}} \sim 10^{22}\,\mathrm{cm^{-2}}$ (Dewangan et al. 2003; Balestra et al. 2004), and *ASCA* observations have indicated the presence of a broad Fe-Kα line of $EW \sim 200\,\mathrm{eV}$ (Weaver et al. 1997, 1998). The line was successfully modeled with a narrow core at the rest-frame energy of 6.4 keV and a broad component superposed on it. This feature was modeled with similar success in the *XMM-Newton* observations of Dewangen et al. and Reeves et al., as well as the *Suzaku* observation also published by these authors (Reeves et al. 2007).

In December 2005, MCG–5-23-16 was simultaneously observed with *XMM-Newton*, *Chandra*, *Suzaku* and *RXTE*. The *XMM-Newton* results are reported by Reeves et al., and our data reduction followed that work (Reeves et al. 2006). The EPIC-pn instrument had a net exposure of 96 ks and returned $\sim 2.2 \times 10^6$ photons after filtering.

As suggested by Reeves et al., a simple photoabsorbed power-law fit does not model the continuum well, especially below $\sim 1\,\mathrm{keV}$. Adding in a source of soft thermal emission also leaves prominent residuals and does not adequately account for the shape of the soft excess, so following the lead of Reeves et al. we have employed a two-power-law model (Reeves et al. 2006): one of the power-law components is affected only by Galactic photoabsorption ($N_{\mathrm{H}} = 8 \times 10^{20}\,\mathrm{cm^{-2}}$ as per Reeves et al.), and hence leaves the AGN system effectively unscattered, while the other component is also subject to absorption intrinsic to the AGN, in this case with a fitted absorbing column density of $N_{\mathrm{H}} = 1.19 \times 10^{22}\,\mathrm{cm^{-2}}$. This component also experiences scattering within the system. We set both power-law photon indices to be equal, indicating that the two power-law components originate from the same physical reservoir of photons (with $\Gamma = 1.66$). Calculating the ratio of the flux of the scattered power-law component to the unscattered power-law component (from $0.6-10.0\,\mathrm{keV}$, fitting only the continuum) yields an estimate of the optical depth of the scattering plasma. In this case $\tau = 7.37 \times 10^{-4}\,\mathrm{ph\,cm^{-2}\,s^{-1}} / 1.83 \times 10^{-2}\,\mathrm{ph\,cm^{-2}\,s^{-1}} \approx 0.04$, so the scattered fraction is low, implying that the electron plasma is optically thin.

The spectrum also shows evidence for two prominent, narrow emission lines of iron Kα and Kβ (at $E_{K\alpha} = 6.4\,\mathrm{keV}$ and $E_{K\beta} = 7.0\,\mathrm{keV}$, with $EW_{K\alpha} = 167\,\mathrm{eV}$ and $EW_{K\beta} = 104\,\mathrm{eV}$, respectively), as well as three narrow absorption lines of intermediately ionized iron at $E_1 = 7.24\,\mathrm{keV}$, $E_2 = 7.48\,\mathrm{keV}$ and $E_3 = 7.85\,\mathrm{keV}$ ($EW_1 = -79\,\mathrm{eV}$, $EW_2 = -121\,\mathrm{eV}$, and $EW_3 = -143\,\mathrm{eV}$, respectively).

After successfully modeling the continuum and narrow line parameters for MCG–5-23-16, we restricted our attention to the hard spectrum ($2.5 - 10.0\,\mathrm{keV}$) and analyzed the broad line component of this source using the method outlined above in §3.2. Note that eliminating soft energies from the fit removed the statistical need for a second, soft power-law in the fit. For a full listing of best-fit model parameters and error bars for MCG–5-23-16, see Table 5. The residual iron line feature, best-fit model and best-fit model components for the hard spectrum are shown in Fig. 2. The best-fitting model for MCG–5-23-16 is the ionized disk reflection spectrum (Ross & Fabian 2005) convolved with `kerrconv`. Although we were not able to constrain the BH spin in this source, we did achieve a fit constraint on the inner radius of the disk emission: $r_{\mathrm{min}} \sim 16 r_{\mathrm{ms}}$. This corresponds to a range of $\sim 36 - 96 r_{\mathrm{g}}$ for a BH spin between $a = 0.0 - 0.998$. Given that the effective inner edge of the disk is not within the radius of marginal stability for a Schwarzschild BH, it is not surprising that we were not able to constrain the value of the BH spin in this source.

A.0.2. NGC 3783

NGC 3783 is a bright, nearby Sy-1 galaxy at a redshift of $z = 0.0097$. It was first detected in X-rays with the *Ariel-V* all-sky survey (McHardy et al. 1981) and subsequently in the high Galactic latitude survey conducted by *HEAO-1* (Piccinotti et al. 1982). Since these early detections, there have been many observations of NGC 3783 with higher resolution instruments: A *ROSAT* observation of the source showed evidence of an ionized absorber in the soft band (Turner et al. 1993), which was confirmed during *ASCA* observations (George et al. 1995, 1998). High-resolution grating observations of NGC 3783 with *Chandra* and *XMM-Newton* followed, unveiling the soft spectrum of this source in detail (Kaspi et al. 2000, 2001, 2002; Blustin et al. 2002; Behar et al. 2003). The higher signal-to-noise of *XMM-Newton*, in particular, has also enabled the iron line to be studied extensively in this source (Reeves et al. 2004). Using two observations from December 2001, Reeves et al. have obtained $\sim 240\,\mathrm{ks}$ of data on NGC 3783. Their global fits to the merged EPIC-pn spectrum are currently second in length and depth only to the $\sim 330\,\mathrm{ks}$ observation of MCG–6-30-15 (Fabian et al. 2002). In these observations, the source has an average $2 - 10\,\mathrm{keV}$ flux of $F_{2-10} = 6.8 \times 10^{-11}\,\mathrm{erg\,cm^{-2}\,s^{-1}}$. The spectrum is noted to have iron line peaks at 6.4 keV and 7.0 keV, representing neutral Fe-Kα ($EW \sim 120\,\mathrm{eV}$) and a blend of ionized Fe-Kα and Fe-Kβ ($EW \sim 35\,\mathrm{eV}$), respectively. A strong absorption line of highly ionized iron is

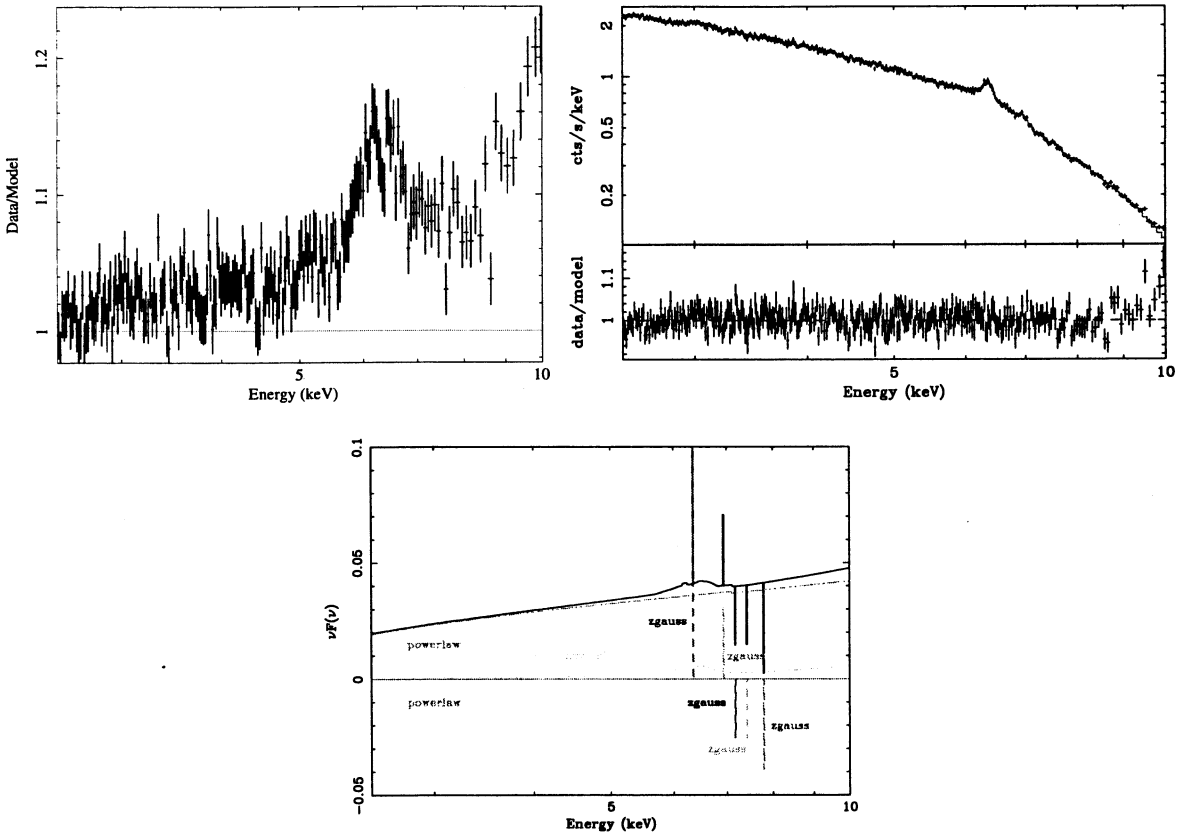

Fig. 2.— *Top left:* The 2.5 – 10.0 keV spectrum of MCG–5-23-16 fit with a two-power-law model modified by Galactic photoabsorption; data-to-model ratio. *Top right:* Best-fit model for MCG–5-23-16, including our continuum model, two narrow emission lines, and five narrow absorption lines as well as an ionized disk reflection spectrum convolved with our `kerrconv` relativistic smearing kernel. *Bottom:* A νF_ν plot depicting the relative flux in each of the best-fit model components in the spectrum.

Model Component	Parameter	Value
phabs	$N_{H1}\,(\mathrm{cm}^{-2})$	8×10^{20}
phabs	$N_{H2}\,(\mathrm{cm}^{-2})$	$1.19^{+0.01}_{-0.01} \times 10^{20}$
po	Γ_{po}	$1.66^{+0.01}_{-0.01}$
	flux (ph cm^{-2} s^{-1})	$1.98^{+0.04}_{-0.13} \times 10^{-2}$
zgauss	E (keV)	6.40
	flux (ph cm^{-2} s^{-1})	$4.00^{+0.35}_{-0.32} \times 10^{-5}$
	EW (eV)	$167.00^{+14.61}_{-13.36}$
zgauss	E (keV)	7.00
	flux (ph cm^{-2} s^{-1})	$9.80^{+2.98}_{-2.87} \times 10^{-6}$
	EW (eV)	$104.00^{+31.62}_{-30.46}$
zgauss	E (keV)	7.24
	flux (ph cm^{-2} s^{-1})	$-7.39^{+2.84}_{-2.73} \times 10^{-6}$
	EW (eV)	$-78.70^{+30.24}_{-29.07}$
zgauss	E (keV)	7.48
	flux (ph cm^{-2} s^{-1})	$-6.93^{+2.83}_{-2.84} \times 10^{-6}$
	EW (eV)	$-121.00^{+49.41}_{-49.59}$
zgauss	E (keV)	7.85
	flux (ph cm^{-2} s^{-1})	$-9.62^{+2.90}_{-2.86} \times 10^{-6}$
	EW (eV)	$-143.00^{+43.11}_{-42.51}$
kerrconv	α_1	$2.45^{+0.59}_{-0.61}$
	α_2	$2.45^{+0.59}_{-0.61}$
	$r_{br}\,(r_{ms})$	6.0
	a	– – –
	$i\,(^\circ)$	$45.88^{+2.34}_{-19.42}$
	$r_{min}\,(r_{ms})$	$15.66^{+13.40}_{-7.33}$
	$r_{max}\,(r_{ms})$	400
reflion	Fe/solar	$0.61^{+0.08}_{-0.05}$
	ξ_{refl} (erg cm^{-1} s^{-1})	< 31.09
	Γ_{refl}	$1.66^{+0.01}_{-0.01}$
	R_{refl}	$0.41^{+0.02}_{-0.02}$
	flux (ph cm^{-2} s^{-1})	$1.64^{+0.10}_{-0.10} \times 10^{-5}$
χ^2/dof		1484/1487 (1.00)

Table 5: Best-fitting model parameters for the 2.5 – 10.0 keV spectrum of MCG–5-23-16, including components and parameter values from 0.6 – 1.5 keV for completeness. The energies from 1.5 – 2.5 keV were not included due to the presence of absorption edges from the *XMM-Newton* mirrors. Error bars are quoted at 90% confidence. For the zgauss lines, we required each to be intrinsically narrow, i.e., $\sigma = 0.0$. Redshifts were frozen at the cosmological value for the source, in this case $z = 0.0085$. Note the absence of warm absorption and a soft excess in this object. When no error bars are quoted, the parameter in question is frozen at the given value.

also observed at 6.67 keV that exhibits variability in direct correlation with that of the continuum flux. A weak red wing of the 6.4 keV line is noted by the authors, but once warm absorption is taken into account in the system the requirements for a broad Fe-Kα component are significantly reduced (Reeves et al. 2004).

We analyzed the first of the two December 2001 *XMM-Newton* observations. We chose not to merge the event files of both data sets to avoid the uncertainties inherent in so doing, instead focusing on only one data set with an effective exposure time of ~ 120 ks and a total of $\sim 1.8 \times 10^6$ photons after filtering. This number of counts is still large enough to obtain valid statistical fits to the model parameters used. We follow the data reduction steps of Reeves et al., excluding the last part of the observation due to contamination from a background flare. Our analysis follows in the same spirit as these authors, but in order to remain consistent with the method described above in §3 we do not make any assumptions about the soft spectrum and continuum emission based on prior RGS results (Blustin et al. 2002).

We begin our analysis of the time-averaged spectrum with a simple photoabsorbed power-law fit using the Galactic absorbing column of $N_{\rm H} = 8.5 \times 10^{20}$ cm^{-2}, and neglecting the energy ranges associated with the mirror edges and the iron lines, as in §3. This fit leaves obvious residuals in all parts of the spectrum, however, and is especially poor for the soft energies below ~ 1.5 keV. Continuum curvature associated with a soft excess and warm absorption are both clearly evident. As discussed by Reeves et al., the fit is much improved with the addition of a thermal blackbody component ($kT \sim 0.07$ keV, as compared with their value: $kT \sim 0.09$ keV). We approach the question of the warm absorption similarly as well, using our XSTAR table model to parameterize the column density and ionization level of the absorbing medium, as do Reeves et al. As with these authors, we find statistical evidence for a two-zone warm absorption structure, though our values for the column densities and ionization parameters of these zones vary significantly from those of Reeves et al. We find $N_{\rm H1} = 6.84 \times 10^{23}$ and $\log\xi_1 < 0.01$, with $N_{\rm H2} = 1.58 \times 10^{23}$ and $\log\xi_2 = 1.40$, whereas Reeves et al. find $N_{\rm H1} = 6.00 \times 10^{20}$ and $\log\xi_1 = 0.30$, with $N_{\rm H2} = 4.60 \times 10^{22}$ and $\log\xi_2 = 2.90$. These differences are not surprising, however, because Reeves et al. base their fits on the RGS results for this source (Blustin et al. 2002). We do not use any *a priori* information to augment or guide the EPIC-pn spectral fits due to calibration uncertainties. Finally, we allowed the value of the neutral hydrogen absorbing column to vary in an effort to improve the goodness-of-fit and found that the spectrum preferred a higher value than the Galactic column: $N_{\rm H} = 3.60 \times 10^{21}$ cm^{-2}. This was also in contrast to the Reeves et al. result, where the cold hydrogen column was held at the Galactic value and not permitted to vary.

Reeves et al. found two emission peaks in the spectrum at 6.4 keV ($EW \sim 120$ eV) and 7.0 keV ($EW \sim 35$ eV), representing cold Fe-Kα and likely a blend of ionized Fe-Kα and Fe-Kβ, respectively. The latter line, in particular, showed no appreciable variance over the observation, leading

the authors to postulate a relatively distant origin for the lines away from the central parts of the accretion disk. A 6.67 keV absorption feature of highly ionized iron was also seen which did appear to vary with time and was strongest when the continuum flux was highest, suggesting an origin in the region of the warm absorber within 0.1 parsec of the nucleus. Though inclusion of the WA and this feature did lessen the statistical case for a broad iron line in NGC 3783, Reeves et al. nonetheless identified a residual broad feature which they fit using a `diskline` model with $\alpha \sim 3.3$, $i \sim 19°$, $r_{\rm min} = 6.0\,r_{\rm g}$, and $EW \sim 58$ eV.

We also detected the emission and absorption features discussed by Reeves et al., though we found that the equivalent widths for the Fe-Kα, Fe-Kα/Kβ blend and ionized iron absorption lines differed from the fits performed by these authors: $EW_{K\alpha} = 79.0$ eV, $EW_{K\alpha/K\beta} = 23.9$ eV and $EW_{\rm abs} = -25.1$ eV. We did not test the time variance of the absorption component because such an examination is beyond the scope of this work. It should also be noted that, contrary to the Reeves et al. analysis, we required the core of the 6.4 keV line to be intrinsically narrow, so it is not unusual that we obtain a smaller equivalent width than Reeves et al. When we included the broad component of the neutral Kα line, the fit improved dramatically. Our best fit to the hard spectrum of NGC 3783 convolved an ionized disk reflection spectrum with `kerrconv`, as can be seen in Table 6 below, but due to the relative narrowness of the iron line we were not able to constrain the BH spin in this source. Not surprisingly, our constraints on the radial extent of the disk showed that $r_{\rm min} < 390\,r_{\rm ms}$, or $< 985\,r_{\rm g}$. A line emitted from so far out in the disk would not exhibit relativistic signatures.

A.0.3. Mrk 766

Mrk 766 is designated as a classic, bright NLS1 galaxy (Sy-1.5) with a redshift of $z = 0.0129$ and a typical $2-10$ keV flux of $F_{2-10} \sim 2.5 \times 10^{-11}$ erg cm^{-2} s^{-1} (Pounds et al. 2003). Previous X-ray observations of this source have provided contradictory evidence on the detection of a broad Fe-Kα feature. Although not one of the most convincing cases, Mrk 766 was included in an *ASCA* spectral survey of bright Seyfert galaxies showing evidence of relativistic iron lines (Nandra et al. 1997). A separate analysis of simultaneous *ROSAT* and *ASCA* observations (Leighly et al. 1996), however, showed the X-ray spectrum to be described by a power-law of index increasing strongly with flux from $\Gamma \sim 1.6$, but with only a narrow Fe-Kα emission line ($EW \sim 100$ eV at 6.4 keV). A later observation with *BeppoSAX* found a steeper power-law ($\Gamma \sim 2.2$), and evidence for an absorption edge at ~ 7.4 keV (Matt et al. 2000), implying strong reflection from intermediately ionized material. Interestingly, based on *XMM-Newton* observations of the source, Turner et al. found that energy-time maps of Mrk 766 reveal a periodic energy shift in an ionized component of Fe-Kα emission, with a period of ~ 165 ks. This can be interpreted as evidence for emission from orbit-

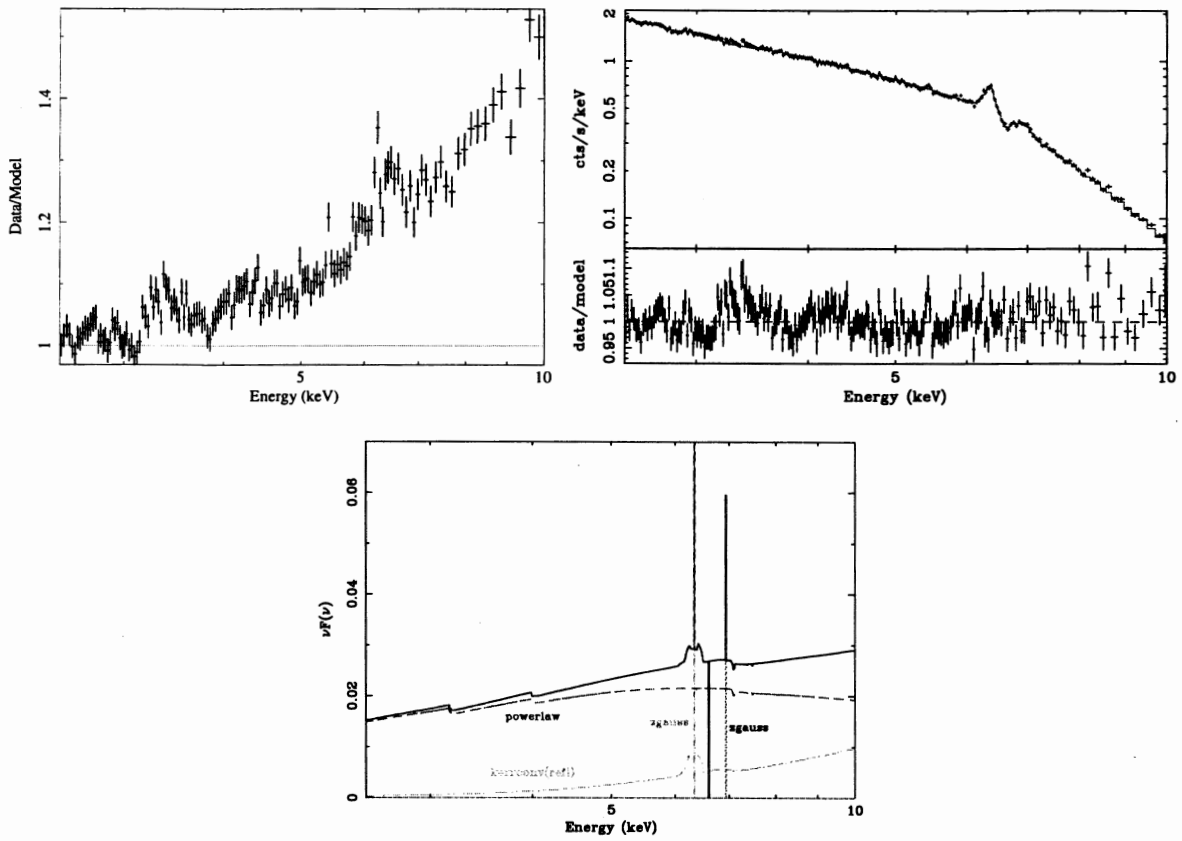

Fig. 3.— *Top left:* The 2.5 – 10.0 keV spectrum of NGC 3783 fit with a power-law model modified by Galactic photoabsorption, along with a two-zone warm absorber and a blackbody soft excess. *Top right:*The 2.5 – 10.0 keV best-fit model for NGC 3783, including our continuum model, two narrow emission lines and a narrow absorption line as well as an ionized disk reflection spectrum convolved with our `kerrconv` relativistic smearing kernel. *Bottom:* A νF_ν plot depicting the relative flux in each of the best-fit model components in the spectrum.

Model Component	Parameter	Value
phabs	$N_{H2}\,(\mathrm{cm}^{-2})$	$3.60^{+0.01}_{-0.01} \times 10^{21}$
WA 1	$N_{WA1}\,(\mathrm{cm}^{-2})$	$6.84^{+0.42}_{-0.20} \times 10^{23}$
	$\log\xi_{WA1}$	< 0.01
WA 2	$N_{WA2}\,(\mathrm{cm}^{-2})$	$1.58^{+0.06}_{-0.04} \times 10^{23}$
	$\log\xi_{WA2}$	$1.40^{+0.04}_{-0.02}$
po	Γ_{po}	$2.50^{+0.02}_{-0.02}$
	flux $(\mathrm{ph\,cm}^{-2}\,\mathrm{s}^{-1})$	$4.60^{+0.09}_{-0.12} \times 10^{-4}$
bbody	kT (keV)	$0.07^{+0.00}_{-0.00}$
	flux $(\mathrm{ph\,cm}^{-2}\,\mathrm{s}^{-1})$	$4.86^{+0.36}_{-0.31} \times 10^{-4}$
zgauss	E (keV)	6.40
	flux $(\mathrm{ph\,cm}^{-2}\,\mathrm{s}^{-1})$	$3.07^{+0.45}_{-0.46} \times 10^{-7}$
	EW (eV)	$79.00^{+11.58}_{-11.84}$
zgauss	E (keV)	7.00
	flux $(\mathrm{ph\,cm}^{-2}\,\mathrm{s}^{-1})$	$8.20^{+2.09}_{-2.05} \times 10^{-8}$
	EW (eV)	$23.90^{+6.44}_{-6.35}$
zgauss	E (keV)	6.67
	flux $(\mathrm{ph\,cm}^{-2}\,\mathrm{s}^{-1})$	$-1.12^{+0.21}_{-0.21} \times 10^{-7}$
	EW (eV)	$-25.10^{+4.71}_{-4.71}$
kerrconv	α_1	$---$
	α_2	$---$
	$r_{br}\,(r_{ms})$	6.0
	a	$---$
	$i\,(^\circ)$	36^{+11}_{-10}
	$r_{min}\,(r_{ms})$	< 391
	$r_{max}\,(r_{ms})$	400
reflion	Fe/solar	$0.19^{+0.03}_{-0.04}$
	$\xi_{refl}\,(\mathrm{erg\,cm}^{-1}\,\mathrm{s}^{-1})$	< 40.10
	Γ_{refl}	$2.50^{+0.02}_{-0.02}$
	R_{refl}	$1.53^{+0.38}_{-0.40}$
	flux $(\mathrm{ph\,cm}^{-2}\,\mathrm{s}^{-1})$	$2.97^{+0.74}_{-0.77} \times 10^{-6}$
χ^2/dof		1526/1486 (1.03)

Table 6: Best-fitting model parameters for the $2.5-10.0$ keV spectrum of NGC 3783, including components and parameter values from $0.6-1.5$ keV for completeness. The energies from $1.5-2.5$ keV were not included due to the presence of absorption edges from the *XMM-Newton* mirrors. Error bars are quoted at 90% confidence. For the zgauss lines, we required each to be intrinsically narrow, i.e., $\sigma = 0.0$. Redshifts were frozen at the cosmological value for the source, in this case $z = 0.0097$. Note the two-zone warm absorber and blackbody soft excess present in this object, similar to many other Sy-1 sources.

ing gas within $\sim 100\,r_g$ of the central BH. A likely explanation is that this gas represents a hot spot on the disk illuminated by magnetic reconnection (Turner et al. 2006).

We examine the May 2001 *XMM-Newton* observation of Mrk 766 taken by Mason et al., from which the RGS results were published in 2003 (Mason et al. 2003) and the EPIC spectra were explored more thoroughly by other authors (Pounds et al. 2003; Turner et al. 2006). In our re-analysis, the EPIC-pn data have an effective exposure time of 128 ks and the filtered data yield $\sim 2.92 \times 10^6$ photons.

Mrk 766 bears many spectral similarities to MCG–6-30-15, showing significant complexity beyond a simple photoabsorbed power-law fit. There is clear evidence for a thermal (`bbody`: $kT = 0.08$ keV) soft excess below ~ 1 keV as well as two distinct physical zones of low ($N_{\rm H1} = 5.26 \times 10^{22}\,{\rm cm}^{-2}$, $\log\xi_1 = 0.21$) to moderately ionized ($N_{\rm H2} = 9.50 \times 10^{23}\,{\rm cm}^{-2}$, $\log\xi_2 = 3.04$) intrinsic absorption. These components exist in addition to cold absorption by the Milky Way ($N_{\rm H} = 1.71 \times 10^{20}\,{\rm cm}^{-2}$). The power-law in this source has a spectral index of $\Gamma = 2.75$, comparable with the result published by Pounds et al. Unfortunately, these authors did not probe the spectrum below 3 keV, so we cannot compare our soft excess or warm absorption parameters to theirs.

The narrow Fe-Kα core of Mrk 766 has a rest-frame energy of 6.4 keV, as expected, and an $EW = 33.7$ eV, again comparable with the findings of Pounds et al. Fitting this line with a Gaussian component leaves significant residuals strongly indicative of the presence of a broad line. This broad component is most successfully fit with a `kerrconv(refl)` model, yielding comparable results to the disk reflection model employed to model the broad iron line in Pounds et al., though with different fit parameters. Our model also detects no absorption features above 8 keV, as discussed by Pounds et al., possibly due to advances in modeling the reflection spectrum. The BH spin, to 90% confidence, is relatively high at $a > 0.85$ and the inner edge of the accretion disk is constrained to $r_{\rm min} < 2.25\,r_{\rm ms}$. The best-fit results are shown in Table 7. Fig. 4 shows the iron line residual, best fit to this residual, and relative contributions of the individual model components, respectively.

A.0.4. 3c273

3c273 is the most distant source in our sample at a redshift of $z = 0.1583$. Classified as a bright variable quasar, this AGN displays a strong jet and during epochs of radio-loudness it possesses the flat X-ray spectrum of a blazar, with highly beamed jet emission (Türler et al. 2006). When the jet is reduced in strength, however, this source has been observed to exhibit Sy-1-type accretion disk signatures such as a broad iron line. A minimum state occurred in March 1986 and allowed Robson et al. (1986) to identify a new near-infrared spectral component. An even better

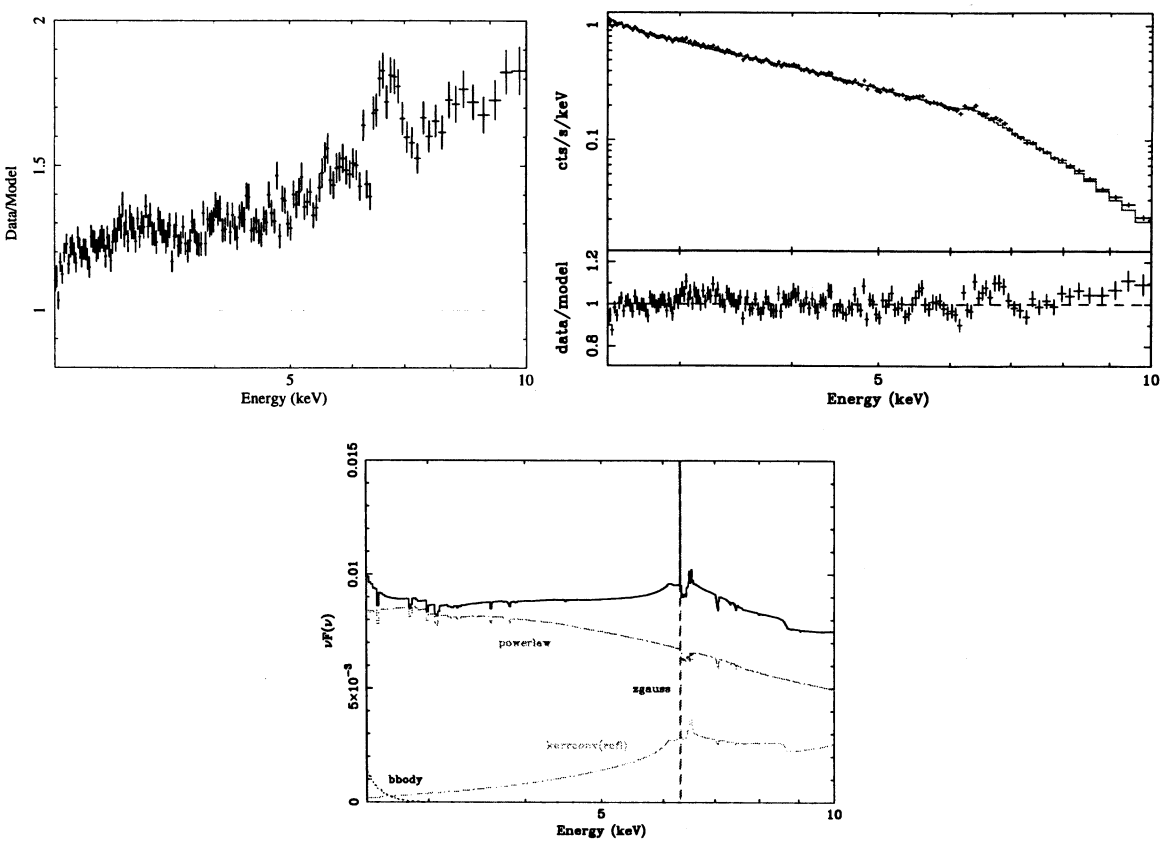

Fig. 4.— *Top left:* The 2.5 – 10.0 keV spectrum of Mrk 766 fit with a continuum composed of a power-law model modified by Galactic photoabsorption, a two-zone warm absorber model and a blackbody soft excess. *Top right:* The 2.5 – 10.0 keV best-fit model for Mrk 766, including our continuum model and an ionized disk reflection spectrum convolved with our `kerrconv` relativistic smearing kernel. *Bottom:* A νF_ν plot depicting the relative flux in each of the model components in the spectrum.

Model Component	Parameter	Value
phabs	$N_{\rm H}\,({\rm cm}^{-2})$	$1.71^{+0.24}_{-0.00} \times 10^{-2}$
WA 1	$N_{\rm WA1}\,({\rm cm}^{-2})$	$5.26^{+0.16}_{-0.31} \times 10^{22}$
	$\log\xi_{\rm WA1}$	$0.21^{+0.01}_{-0.03}$
WA 2	$N_{\rm WA2}\,({\rm cm}^{-2})$	$9.50^{+0.05}_{-0.02} \times 10^{23}$
	$\log\xi_{\rm WA2}$	$3.04^{+0.08}_{-0.07}$
po	$\Gamma_{\rm po}$	$2.75^{+0.05}_{-0.06}$
	flux $({\rm ph\,cm^{-2}\,s^{-1}})$	$2.05^{+0.08}_{-0.12} \times 10^{-4}$
bbody	$kT\,({\rm keV})$	$0.08^{+0.00}_{-0.00}$
	flux $({\rm ph\,cm^{-2}\,s^{-1}})$	$1.88^{+0.32}_{-0.26} \times 10^{-6}$
zgauss	E (keV)	6.40
	flux $({\rm ph\,cm^{-2}\,s^{-1}})$	$4.71^{+1.35}_{-1.90} \times 10^{-8}$
	EW (eV)	$33.70^{+9.66}_{-13.59}$
kerrconv	α_1	$1.93^{+0.15}_{-0.13}$
	α_2	$1.93^{+0.15}_{-0.13}$
	$r_{\rm br}\,(r_{\rm ms})$	6.0
	a	$0.99^{+0.01}_{-0.14}$
	$i\,(^\circ)$	74^{+7}_{-1}
	$r_{\rm min}\,(r_{\rm ms})$	< 2.25
	$r_{\rm max}\,(r_{\rm ms})$	400
reflion	Fe/solar	1.0
	$\xi_{\rm refl}\,({\rm erg\,cm^{-1}\,s^{-1}})$	579^{+274}_{-134}
	$\Gamma_{\rm refl}$	$2.75^{+0.05}_{-0.06}$
	$R_{\rm refl}$	$2.54^{+0.32}_{-0.32}$
	flux $({\rm ph\,cm^{-2}\,s^{-1}})$	$8.29^{+1.05}_{-1.05} \times 10^{-6}$
χ^2/dof		1492/1309 (1.14)

Table 7: Best-fitting model parameters for the $2.5-10.0$ keV spectrum of Mrk 766, including components and parameter values from $0.6-1.5$ keV for completeness. The energies from $1.5-2.5$ keV were not included due to the presence of absorption edges from the *XMM-Newton* mirrors. Error bars are quoted at 90% confidence. We required the zgauss line representing the core of the Fe-Kα feature to be intrinsically narrow, i.e., $\sigma = 0.0$. Redshifts were frozen at the cosmological value for the source, in this case $z = 0.0130$. A two-zone warm absorber and blackbody soft excess are present in this object, as in MCG–6-30-15 and many other Sy-1 sources.

opportunity arose in early 2004, when the sub-millimeter flux of 3c273 was observed to be almost two times lower than in 1986. This new minimum triggered a slew of simultaneous observations with instruments in all wavebands such as *INTEGRAL*, *XMM-Newton* and *RXTE*, among several other optical, radio and sub-millimeter telescopes. The $2-10\,\mathrm{keV}$ flux during this period was $F_{2-10} = 6.7 \times 10^{-11}\,\mathrm{erg\,cm^{-2}\,s^{-1}}$. Such a low flux in 3c273 has only been measured twice in the past, by *Ginga* in July 1987 (Turner et al. 1990) and by *BeppoSAX* on 18 July 1996 (Haardt et al. 1998), the latter of which was coincident with the low sub-mm flux mentioned above. This X-ray/sub-mm correlation strongly supports a synchrotron self-Compton origin for the X-ray jet emission in 3c273.

Türler et al. obtained a 20 ks *XMM-Newton* observation of 3c273 during this jet-minimum state in June 2004. We use their thin-filter EPIC-pn observation in the interest of collecting as many photons as possible, though due to photon pile-up it is necessary to exclude the centralmost region of the source, as detailed by the authors (Türler et al. 2006). In our filtered data set we capture $\sim 7.5 \times 10^5$ photons.

Türler et al. note the inadequacy of a simple photoabsorbed power-law fit to the data. Their best fit to the continuum is achieved using two power-law components: $\Gamma_{\mathrm{hard}} = 1.63 \pm 0.02$ and $\Gamma_{\mathrm{soft}} = 2.69 \pm 0.06$, with the hard component flux ~ 2.3 times the soft flux. Both components were modified by Galactic photoabsorption with $N_{\mathrm{H}} = 1.79 \times 10^{20}\,\mathrm{cm^{-2}}$. We based our initial continuum fit on theirs, with two power-law components: $\Gamma_{\mathrm{hard}} = 1.72^{+0.11}_{-0.28}$ and $\Gamma_{\mathrm{soft}} = 3.01^{+1.29}_{-0.71}$, both consistent with the Türler et al. results. The ratio we calculate between the fluxes of the hard and soft power-law components is 4.18, however. This is significantly higher than that calculated by Türler et al., and the error bars on the spectral indices, in particular, led us to consider eliminating the soft component. Our best-fitting continuum model, therefore, has only one power-law component at $\Gamma = 2.03$ and exhibits the same statistical goodness-of-fit as the two power-law model.

Evidence for excess emission from $2.5-7.0\,\mathrm{keV}$ was also found by Türler et al., supporting the presence of a broad Fe-Kα line when 3c273 is in a jet-minimum state. The authors quote this excess as significant at the 6σ level with an integrated flux of $2.6 \pm 0.4 \times 10^{-4}\,\mathrm{ph\,cm^{-2}\,s^{-1}}$, corresponding to an $EW = 166 \pm 26\,\mathrm{eV}$. These values are consistent with those reported from previous observations of the source in a jet-minimum state (Kataoka et al. 2002; Page et al. 2004; Yaqoob & Serlemitsos 2000). The breadth of the excess is not satisfactorily fitted by a Gaussian line or a `diskline` component from a non-rotating BH. If the line extent is real, the only remaining explanation, according to the authors, is that it is emitted from around a near-extreme Kerr BH. The sharp edge of the iron line at 7 keV suggests that the angle of inclination of the accretion disk is $35-40°$ (Türler et al. 2006).

We find evidence for a similar excess around the Fe-Kα line in our analysis. Interestingly, we do *not* see a narrow emission line at 6.4 keV, but rather the narrow line core seems to coincide

with the He-like line of Fe-Kα at 6.66 keV with an $EW = 73.3$ eV. This may mean that the gas in this system is highly ionized, which would not be surprising in such an active source. Visually, the residuals left over after fitting this narrow line suggest the presence of a broad component. Modeling this component with our analysis method provides a modest improvement in the global goodness-of-fit compared with other sources, perhaps due to the distance of the source and the paucity of the data. With a 20 ks observation we have collected $< 3 \times 10^5$ photons from $2.5 - 10$ keV. Given more observing time and a larger number of (pile-up free) photons, our line analysis would be significantly improved. Taking into account these caveats about the robustness of the broad line, our `kerrconv(refl)` model still provides the best fit, as shown in Table 8. Fig. 5 shows the iron line residual, best fit to this residual, and relative contributions of the individual model components in the best fit, respectively. To 90% confidence, $a > 0.72$ and $r_{\rm min} < 2.30 r_{\rm ms}$, but longer, more sensitive observations are necessary in order to further substantiate these results.

A.0.5. NGC 2992

NGC 2992 is a Sy-1.9 galaxy that appears to show a broad iron line even though it is highly obscured. This source has been the subject of intense study due to the variability of its X-ray emission (Gilli et al. 2000). In 1997 and 1998, *BeppoSAX* caught NGC 2992 transitioning from a Compton-thick to a Compton-thin state, resulting in an order of magnitude increase in its X-ray luminosity as well as a qualitative difference in its spectral appearance, with more disk features (e.g., broad lines) being seen in several wavelengths. The source has a redshift of $z = 0.0077$. In the two *BeppoSAX* pointings, NGC 2992 displays a $2 - 10$ keV X-ray fluxes of 0.63 and 7.4×10^{-11} erg cm^{-2} s^{-1} (Gilli et al. 2000).

We use the May 2003 *XMM-Newton* observation of NGC 2992, totaling 29 ks, which translates to $\sim 6.02 \times 10^5$ photons in the filtered data set. This observation appears to be unpublished, so all the fit values referenced herein are our own, compiled using the reduction and analysis methods detailed in §3.

Upon first inspection, it is immediately clear that NGC 2992 is heavily absorbed below ~ 2 keV. Though statistical evidence exists for a soft excess, none of the telltale signatures of intrinsic warm absorption are present, and the flux decreases precipitously at soft energies. When a simple photoabsorbed power-law model plus blackbody emission is applied to the continuum, the remaining residuals on the soft end indicate that some absorption remains unaccounted for, but allowing the column density of hydrogen to fit freely above the Galactic value of $N_{\rm H} = 5.26 \times 10^{20}$ cm^{-2} neatly corrects the discrepancy. The final continuum parameters are $N_{\rm H} = 5.11 \times 10^{21}$ cm^{-2}, $\Gamma = 1.69$ and $kT = 0.05$ keV with the power-law flux 1.4 times greater than that of the blackbody component.

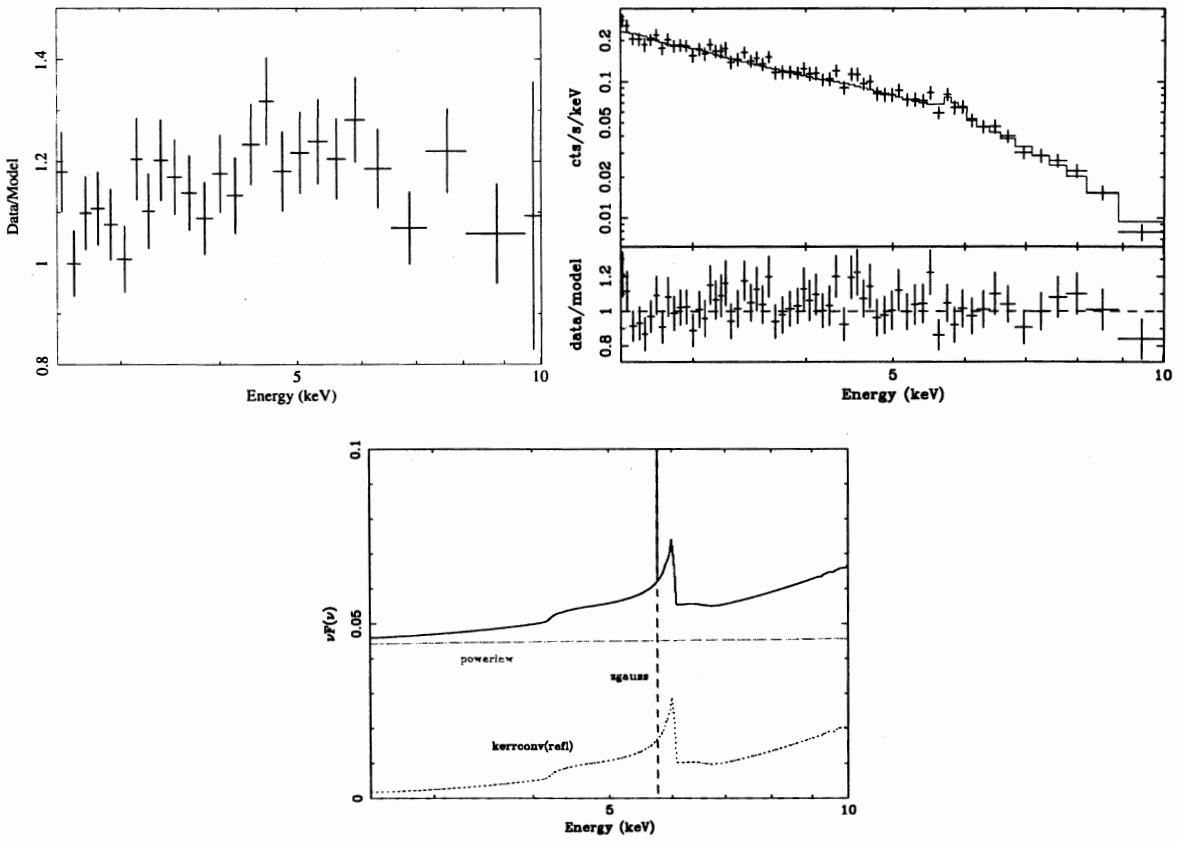

Fig. 5.— *Top left:* The 2.5 – 10.0 keV spectrum of 3c273 fit with a power-law model modified by Galactic photoabsorption. *Top right:* The 2.5 – 10.0 keV best-fit model for 3c273, including our continuum model and an ionized disk reflection spectrum convolved with our `kerrconv` relativistic smearing kernel. *Bottom:* A νF_ν plot depicting the relative flux in each of the model components in the spectrum.

Model Component	Parameter	Value
phabs	$N_{\rm H}\,({\rm cm}^{-2})$	$1.79^{+1.88}_{-0.00} \times 10^{-2}$
po	$\Gamma_{\rm po}$	$2.03^{+0.30}_{-0.12}$
	flux (ph cm^{-2} s^{-1})	$3.82^{+0.47}_{-0.83} \times 10^{-2}$
zgauss	E (keV)	6.66
	flux (ph cm^{-2} s^{-1})	$9.30^{+0.76}_{-0.75} \times 10^{-5}$
	EW (eV)	$73.30^{+5.99}_{-5.91}$
kerrconv	α_1	$4.22^{+1.78}_{-1.48}$
	α_2	$4.22^{+1.78}_{-1.48}$
	$r_{\rm br}\,(r_{\rm ms})$	6.0
	a	> 0.72
	$i\,(^\circ)$	< 63
	$r_{\rm min}\,(r_{\rm ms})$	< 2.30
	$r_{\rm max}\,(r_{\rm ms})$	400
refl	Fe/solar	1.0
	$\xi_{\rm refl}$ (erg cm^{-1} s^{-1})	< 355.88
	$\Gamma_{\rm refl}$	$2.03^{+0.30}_{-0.12}$
	$R_{\rm refl}$	$4.76^{+28.34}_{-3.84}$
	flux (ph cm^{-2} s^{-1})	$1.70^{+10.12}_{-1.37} \times 10^{-4}$
χ^2/dof		288/265 (0.86)

Table 8: Best-fitting model parameters for the $2.5-10.0$ keV spectrum of 3c273, including components and parameter values from $0.6-1.5$ keV for completeness. The energies from $1.5-2.5$ keV were not included due to the presence of absorption edges from the *XMM-Newton* mirrors. Error bars are quoted at 90% confidence. We required the zgauss line representing the core of the Fe-Kα feature to be intrinsically narrow, i.e., $\sigma = 0.0$. Interestingly, this line was found at a moderate ionization state of iron (6.66 keV) rather than at the neutral rest-frame energy of 6.4 keV. Redshifts were frozen at the cosmological value for the source, in this case $z = 0.1583$. No warm absorption or soft excess is seen in this object. Note the large error bars on the value of $R_{\rm refl}$ that we calculate. These are likely an artifact of the relatively low photon count for this observation.

The Fe-Kα line is present with a narrow core at 6.4 keV and $EW = 38.8$ eV. Significant residuals remain surrounding the core, however, and the best statistical fit is achieved with a `kerrconv(refl)` model. See Table 9 for model parameters and error bars. Fig. 6 shows the iron line residual, best fit to this residual, and relative contributions of the individual model components for the best fit. Note that the BH spin cannot be constrained. Constraints are also difficult to achieve on the disk emissivity index α, especially, though we have constrained the effective inner disk radius to $r_{\rm min} < 11.78 r_{\rm ms}$. These large error bars are seen due to the paucity of photons in the hard band ($2.5 - 10$ keV) in this observation: with only 29 ks and a flux of $F_{2.5-10} = 8.06 \times 10^{-11}$ erg cm^{-2} s^{-1}, we have $< 2 \times 10^5$ photons to use in spectral fitting. This is only a small fraction ($< 20\%$) of the number of counts we have at our disposal for the same energy range in MCG–6-30-15, so it is not surprising that our statistics are not as sound in this case.

A.0.6. NGC 4051

NGC 4051, like NGC 2992, is a heavily absorbed Seyfert AGN (Sy-1.5; NLS1) seen to vary significantly in flux over the course of several observations (Guainazzi et al. 1996; Lamer et al. 2003). The source is at a redshift of $z = 0.0023$ and has a typical flux on the order of a few times 10^{-11} erg cm^{-2} s^{-1}, though as stated above, this flux can vary significantly on a variety of time scales, along with the spectral characteristics of the source. Unusually low flux states in this object can last for weeks to months, during which time the X-ray spectrum shows a hard continuum power-law of spectral slope $\Gamma \sim 1$, but is dominated by a softer component at lower energies with $\Gamma \sim 3$ (Uttley et al. 2004). A highly broadened and redshifted iron line has also been noted in the low flux state of NGC 4051 with *RXTE*, suggesting that reflection features from the accretion disk close to the BH may remain constant in this source in spite of the large variations in continuum properties (Uttley et al. 2003).

NGC 4051 was observed with *XMM-Newton* in May 2001 for a duration of 117 ks, yielding $\sim 3.27 \times 10^6$ photons in the filtered data set. The EPIC-pn results were first reported by Mason et al., and suggested a continuum described by a power-law "pivoting" around 100 keV, according to a simultaneous observation with *RXTE*. Ultraviolet emission from the Optical Monitor on *XMM-Newton* was found to lag the X-ray emission by ~ 0.2 days, indicating that it is likely reprocessed X-ray emission. The X-ray emission itself showed variability on time scales as small as $1 - 2$ hours (Mason et al. 2002). These results were expanded upon by Pounds et al., who noted the intermediate flux of the source at this time and validated the presence of both an iron line and a thermal soft excess during the May 2001 observation (Pounds et al. 2004). Ponti et al. recently re-analyzed this observation as well as a lower-flux pointing from November 2002 and reinforced the veracity of this model, while also considering the comparable efficacy of a model dominated

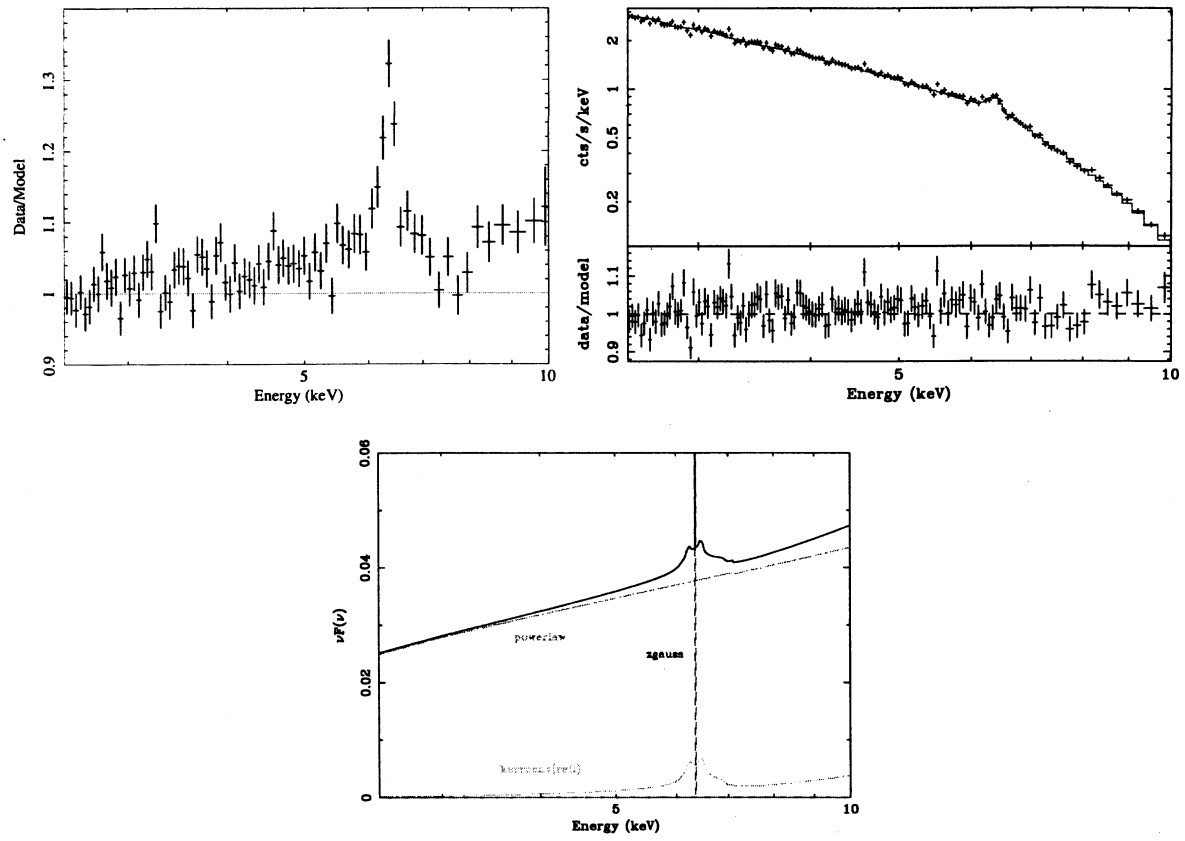

Fig. 6.— *Top left:* The 2.5 – 10.0 keV spectrum of NGC 2992 fit with a continuum composed of a power-law model modified by Galactic photoabsorption as well as a blackbody soft excess. *Top right*: The 2.5 – 10.0 keV best-fit model for NGC 2992, including our continuum model and an ionized disk reflection spectrum convolved with our `kerrconv` relativistic smearing kernel. *Bottom:* A νF_ν plot depicting the relative flux in each of the model components in the spectrum.

Model Component	Parameter	Value
phabs	$N_{\rm H}\,(\,{\rm cm}^{-2}\,)$	$5.12^{+0.09}_{-0.10} \times 10^{21}$
po	$\Gamma_{\rm po}$	$1.69^{+0.02}_{-0.03}$
	flux $(\,{\rm ph\,cm}^{-2}\,{\rm s}^{-1}\,)$	$2.14^{+0.08}_{-0.07} \times 10^{-2}$
bbody	$kT\,({\rm keV})$	$0.05^{+0.01}_{-0.01}$
	flux $(\,{\rm ph\,cm}^{-2}\,{\rm s}^{-1}\,)$	$1.53^{+5.01}_{-0.93} \times 10^{-2}$
zgauss	E (keV)	6.40
	flux $(\,{\rm ph\,cm}^{-2}\,{\rm s}^{-1}\,)$	$1.85^{+2.32}_{-1.54} \times 10^{-5}$
	EW (eV)	$38.80^{+48.66}_{-32.30}$
kerrconv	α_1	$7.36^{+2.64}_{-6.12}$
	α_2	$7.36^{+2.64}_{-6.12}$
	$r_{\rm br}\,(r_{\rm ms})$	6.0
	a	$---$
	$i\,(^\circ)$	41^{+7}_{-21}
	$r_{\rm min}\,(r_{\rm ms})$	$2.50^{+9.28}_{-1.50}$
	$r_{\rm max}\,(r_{\rm ms})$	400
reflion	Fe/solar	1.0
	$\xi_{\rm refl}\,(\,{\rm erg\,cm}^{-1}\,{\rm s}^{-1}\,)$	30.0
	$\Gamma_{\rm refl}$	$1.69^{+0.02}_{-0.03}$
	$R_{\rm refl}$	$0.64^{+0.22}_{-0.20}$
	flux $(\,{\rm ph\,cm}^{-2}\,{\rm s}^{-1}\,)$	$2.49^{+0.85}_{-0.77} \times 10^{-5}$
χ^2/dof		1402/1312 (1.07)

Table 9: Best-fitting model parameters for the $2.5-10.0\,{\rm keV}$ spectrum of NGC 2992, including components and parameter values from $0.6-1.5\,{\rm keV}$ for completeness. The energies from $1.5-2.5\,{\rm keV}$ were not included due to the presence of absorption edges from the *XMM-Newton* mirrors. Error bars are quoted at 90% confidence. We required the 6.4 keV zgauss line core to be intrinsically narrow, i.e., $\sigma = 0.0$. Redshifts were frozen at the cosmological value for the source, in this case $z = 0.0077$. No evidence for warm absorption is detected, though a soft excess is found in this object, as in many other Sy-1 sources.

by ionized reflection from radii quite close to the BH (Ponti et al. 2006).

We have also focused on the May 2001 observation of NGC 4051, following the reduction and analysis of Mason et al. and Ponti et al. but using modern calibration files. A two power-law model parameterized the continuum with much greater accuracy than either a single power-law, a broken power-law or a "pivoting" power-law of the type employed in previous X-ray spectral analyses. Hard and soft components were detected: $\Gamma_{\rm hard} = 2.01$ and $\Gamma_{\rm soft} = 5.20$. The hard/soft flux ratio for these components is 1.21, and each is modified by photoabsorption from neutral hydrogen with $N_{\rm H} = 7.63 \times 10^{20}\,{\rm cm}^{-2}$. This column density is greater than the Galactic value by a factor of ~ 6, indicating the presence of cold absorption within the NGC 4051 system. Additionally, there is statistical evidence to support the presence of a warm absorber within the AGN as well: a significant improvement in the global goodness-of-fit is seen with the inclusion of one of our XSTAR multiplicative table models with a hydrogen column density of $N_{\rm WA} = 5.08 \times 10^{22}\,{\rm cm}^{-2}$ and $\log\xi_{\rm WA} = 0.06$. Note that this warm absorber is essentially neutral, implying that it does not experience significant heating from the central engine and may exist at some distance from the source of the X-ray emission in NGC 4051. Finally, a soft excess is also seen below ~ 1 keV, as in so many other Seyfert galaxies. The best fit to this feature is achieved with a thermal blackbody component, with $kT = 0.27$ and a flux ~ 120 times smaller than the hard power-law component.

A narrow 6.4 keV Gaussian was successfully fit to the core of the Fe-Kα line in this source, though by forcing the line to be narrow (i.e., freezing $\sigma = 0.0$) we note significant residuals marking the red and blue wings of the broadened line. The narrow core has an $EW = 57.8$ eV. The remaining broad line is best fit with a `kerrconv(refl)` model having a BH spin of $a > 0.67$ and an $r_{\rm min} = 2.25 - 4.62\,r_{\rm ms}$. Full parameter values and 90% confidence error bars are listed in Table 10. Fig. 7 shows the iron line residual, best fit to this residual, and relative contributions of the individual model components, respectively.

A.0.7. Ark 120

Ark 120 is a bright Sy-1 AGN with an estimated BH mass of $\sim 2 \times 10^8\,{\rm M}_\odot$ (Wandel et al. 1999) and a bolometric luminosity of $L_{\rm bol} \geq 10^{45}\,{\rm erg\,s}^{-1}$ (Edelson & Malkan 1986). At a redshift of $z = 0.0327$, this source has a relatively constant $2 - 10$ keV X-ray flux of $F_{2-10} \sim 2.50 \times 10^{-11}\,{\rm erg\,cm}^{-2}\,{\rm s}^{-1}$ (Vaughan et al. 2004). The source is radio-quiet, and due to a lack of observed evidence for intrinsic absorption, Ark 120 has been labeled a "bare" Sy-1 nucleus (Ward et al. 1987; Vaughan et al. 2004). Its host galaxy is an early-type spiral of Hubble type S0/a with an inclination angle of $i \approx 26^\circ$ (Nordgren et al. 1995). Ark 120 has been observed by most of the major X-ray observatories. An *EXOSAT* observation showed the source to have a steep soft X-ray spectrum (Turner & Pounds 1989), as did a subsequent *ROSAT* observation (Brandt et al. 1993).

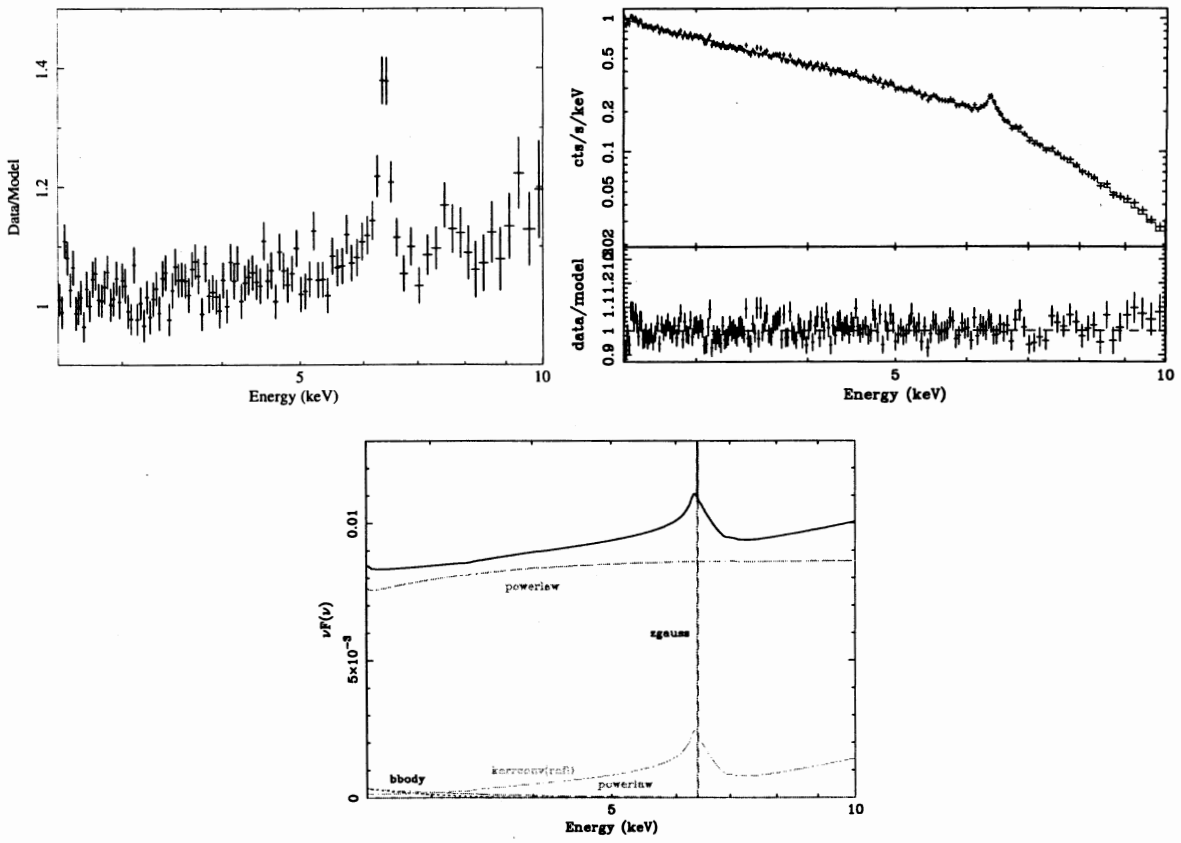

Fig. 7.— *Top left:* The 2.5 – 10.0 keV spectrum of NGC 4051 fit with a continuum composed of two power-law models modified by Galactic photoabsorption, a warm absorber model and a blackbody soft excess. *Top right:* The 2.5 – 10.0 keV best-fit model for NGC 4051, including our continuum model and an ionized disk reflection spectrum convolved with our `kerrconv` relativistic smearing kernel. *Bottom:* A νF_ν plot depicting the relative flux in each of the model components in the spectrum.

Model Component	Parameter	Value
phabs	$N_{\rm H}\,(\,{\rm cm}^{-2}\,)$	$7.63^{+1.97}_{-3.29}\times10^{20}$
WA	$N_{\rm WA}\,(\,{\rm cm}^{-2}\,)$	$5.08^{+0.83}_{-0.72}\times10^{22}$
	$\log\xi_{\rm WA}$	<0.06
po	$\Gamma_{\rm po}$	$5.20^{+0.12}_{-0.35}$
	flux $(\,{\rm ph\,cm}^{-2}\,{\rm s}^{-1}\,)$	$6.13^{+0.61}_{-0.58}\times10^{-4}$
po	$\Gamma_{\rm po}$	$2.01^{+0.08}_{-0.06}$
	flux $(\,{\rm ph\,cm}^{-2}\,{\rm s}^{-1}\,)$	$7.43^{+0.51}_{-0.47}\times10^{-4}$
bbody	$kT\,({\rm keV})$	$0.27^{+0.02}_{-0.01}$
	flux $(\,{\rm ph\,cm}^{-2}\,{\rm s}^{-1}\,)$	$6.31^{+1.29}_{-1.14}\times10^{-6}$
zgauss	E (keV)	6.40
	flux $(\,{\rm ph\,cm}^{-2}\,{\rm s}^{-1}\,)$	$1.05^{+0.33}_{-0.31}\times10^{-6}$
	EW (eV)	$57.80^{+18.17}_{-17.06}$
kerrconv	α_1	$6.78^{+3.22}_{-2.55}$
	α_2	$6.78^{+3.22}_{-2.55}$
	$r_{\rm br}\,(r_{\rm ms})$	6.0
	a	$0.98^{+0.01}_{-0.31}$
	$i\,(^\circ)$	38^{+3}_{-3}
	$r_{\rm min}\,(r_{\rm ms})$	$3.37^{+1.25}_{-1.13}$
	$r_{\rm max}\,(r_{\rm ms})$	400
reflion	Fe/solar	$1.89^{+3.80}_{-0.64}$
	$\xi_{\rm refl}\,(\,{\rm erg\,cm}^{-1}\,{\rm s}^{-1}\,)$	<107.77
	$\Gamma_{\rm refl}$	$2.01^{+0.08}_{-0.06}$
	$R_{\rm refl}$	$1.09^{+0.91}_{-0.81}$
	flux $(\,{\rm ph\,cm}^{-2}\,{\rm s}^{-1}\,)$	$7.55^{+6.28}_{-5.56}\times10^{-7}$
χ^2/dof		1475/1394 (1.06)

Table 10: Best-fitting model parameters for the $2.5-10.0$ keV spectrum of NGC 4051, including components and parameter values from $0.6-1.5$ keV for completeness. The energies from $1.5-2.5$ keV were not included due to the presence of absorption edges from the *XMM-Newton* mirrors. Error bars are quoted at 90% confidence. We required the 6.4 keV zgauss line to be intrinsically narrow, i.e., $\sigma=0.0$. Redshifts were frozen at the cosmological value for the source, in this case $z=0.0023$. A warm absorber and blackbody soft excess are present in this object, as in many other Sy-1 sources.

Furthermore, as mentioned above, these X-ray observations showed no indication of any warm absorption features. Similar findings were seen in ultraviolet observations (Crenshaw et al. 1999; Crenshaw & Kraemer 2001).

The source was observed by *XMM-Newton* in August 2003 for an effective duration of 100 ks ($\sim 2.74 \times 10^6$ photons) by Vaughan et al., whose results on the EPIC-pn spectrum were reported the following year. We follow the data reduction and analysis of these authors, though we restrict our attention to the EPIC-pn camera data. Vaughan et al. find that the continuum emission is well described by a simple photoabsorbed power-law model with no evidence for complex absorption intrinsic to the system. This finding is substantiated by a comparison to the spectrum of 3c273 in its radio-loud state, when the source is dominated by jet emission and displays a very flat, featureless X-ray spectrum lacking intrinsic emission and absorption features. Vaughan et al. calculated the ratio between the spectra of Ark 120 and 3c273, then normalized it by a spectral model for 3c273. The resulting spectrum clearly shows that Ark 120, too, possesses a flat, featureless continuum above ~ 1 keV and that its only significant emission line is that of Fe-Kα at 6.4 keV. The authors use a multiple blackbody component for the soft excess to reduce residuals left over from the power-law fit below ~ 1 keV, and a slight curvature of the continuum is noted that is thought to indicate the presence of disk reflection in this source (Vaughan et al. 2004).

Our continuum fit differs from that of Vaughan et al., most notably over whether or not a warm absorber is present at low energies. These authors relied heavily upon the RGS data to draw their conclusions about the X-ray spectrum of Ark 120 below ~ 3 keV, whereas we use only the EPIC-pn spectrum to produce our global fits to avoid dealing with the calibration problems that exist between the two instruments, as discussed in previous Sections. We do find a similar photoabsorbed power-law, however: $\Gamma = 2.25$ and $N_{\rm H} = 1.26 \times 10^{21}\,{\rm cm}^{-2}$ (the Galactic value, with no evidence for intrinsic cold absorption in the AGN). We detect the presence of a two-zone warm absorber in the system with hydrogen column densities of $N_1 = 1.51 \times 10^{23}\,{\rm cm}^{-2}$, $N_2 = 2.90 \times 10^{22}\,{\rm cm}^{-2}$ and ionization parameters of $\log\xi_1 = 2.97$ and $\log\xi_2 = 1.24$. Our best fit to the soft excess required one blackbody component of $kT = 0.13$ keV and a flux of $F_{\rm bb} = 1.95 \times 10^{-6}\,{\rm ph\,cm^{-2}\,s^{-1}}$, a factor of 60 below the flux of the power-law component. It should be noted that adding in the first WA table resulted in a $\Delta\chi^2/{\rm dof} = -838/+2$, and adding in the second table further improved the fit by $\Delta\chi^2/{\rm dof} = -1163/+2$. The blackbody component resulted in $\Delta\chi^2/{\rm dof} = -4416/+2$. All of these additions to the global fit are therefore statistically warranted.

Vaughan et al. detected the presence of broad and narrow components to the 6.4 keV Fe-Kα line ($EW_{\rm broad} \sim 100$ eV, $EW_{\rm narrow} \sim 40$ eV). The narrow component could easily be fit with a 6.4 keV Gaussian profile, as was our Fe-Kα narrow core, but Vaughan et al. found that a `diskline` model worked best for their broad component ($r_{\rm min} \approx 144\,r_{\rm g}$). Interestingly, this broad component fit to a rest-frame energy of 6.56 keV rather than 6.4 keV, with the latter yielding a substantially

worse global fit ($\Delta\chi^2 = +21.5$) (Vaughan et al. 2004). This energy corresponds to the line emission being dominated by mildly ionized iron (Fe XX-XXII), meaning that resonant trapping and the Auger effect should destroy the line (Ross et al. 1996).

In an effort to solve this puzzle we have fit our iron line profile with two narrow Gaussian components, one at 6.4 keV and one at 6.97 keV, representing neutral and highly ionized iron. The lines have $EW_{\rm cold} = 54.4$ eV and $EW_{\rm ionized} = 19.9$ eV. This fit leaves a residual broad feature nicely centered at 6.4 keV, which renders this scenario physically consistent with other systems and removes the need to explain the presence of the broad line of iron in an intermediate state of ionization. We then achieve a best fit to the broad component using a `kerrconv(refl)` model, which also nicely accounts for the additional curvature noted in the spectrum by Vaughan et al. From this fit, we have constrained the spin of the BH to be $a = 0.63 - 0.68$ and $r_{\rm min} = 1.00 - 1.09\,r_{\rm ms}$. The best-fit parameter values and error bars are presented in Table 11. Fig. 8 shows the iron line residual, best fit to this residual, and relative contributions of the individual model components for the best fit.

Though this result is intriguing for its intermediate BH spin value, one must interpret it with caution. This source, in particular, seems to have a weak emission feature present in the spectrum just below the neutral iron line in energy that sticks out as a "bump" in the spectrum. It is unclear what this feature may represent, and left unmodeled, the spectral fit seems to smooth over it rather than fit it properly. This may affect the parameter values and error bars we obtain for the `kerrconv(refl)` model. More detailed, longer observations with higher spectral resolution will be required to solve this puzzle and more reliably determine the BH spin in Ark 120.

A.0.8. Fairall 9

Fairall 9 is a radio-quiet Sy-1 type galaxy with an elliptical companion, both at a moderate redshift of $z = 0.047$. This source has not been observed to undergo very large changes in X-ray flux over the time it has been observed: the typical $2 - 10$ keV flux of Fairall 9 is $F_{2-10} \sim 1.5 - 5.0 \times 10^{-11}$ erg cm^{-2} s^{-1} (Reynolds 1997; Gondoin et al. 2001). Previous X-ray observations with *ASCA* show that the source has a continuum well-described by a photoabsorbed power-law with a fluorescent Fe-Kα line and a high-energy tail (a common signature of disk reflection, as has been discussed previously with respect to a number of other sources in this Section) (Reynolds 1997; Nandra et al. 1997). A soft excess has also been detected below ~ 2 keV (Pounds et al. 1994), though no strong evidence of warm absorption has been observed in the soft spectrum (Gondoin et al. 2001).

The source was observed with *XMM-Newton* by Jansen et al. in July 2000 for an effective du-

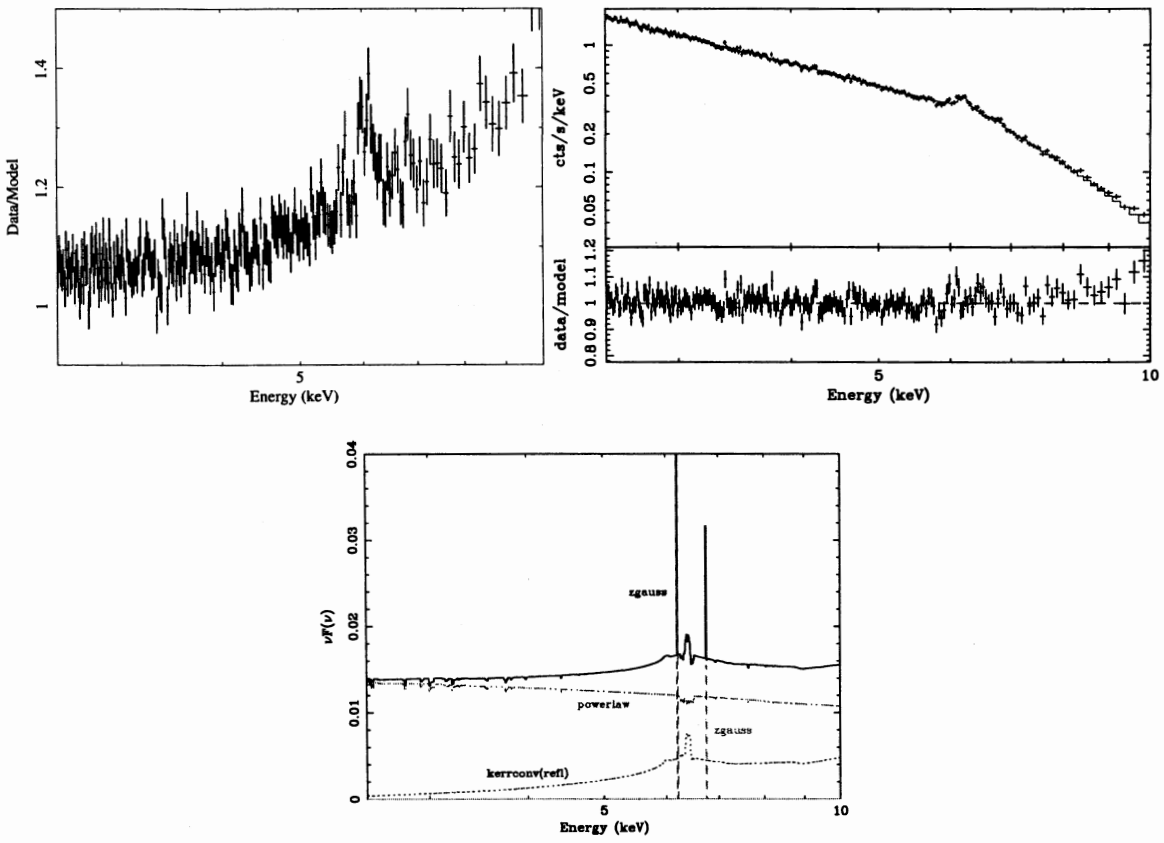

Fig. 8.— *Top left:* The 2.5 – 10.0 keV spectrum of Ark 120 fit with a continuum composed of a power-law model modified by Galactic photoabsorption, a two-zone warm absorber model and a blackbody soft excess. *Top right:* The 2.5 – 10.0 keV best-fit model for Ark 120, including our continuum model and an ionized disk reflection spectrum convolved with our `kerrconv` relativistic smearing kernel. *Bottom:* A νF_ν plot depicting the relative flux in each of the model components in the spectrum.

Model Component	Parameter	Value
phabs	$N_{\rm H}\,(\,{\rm cm}^{-2}\,)$	1.26×10^{21}
WA 1	$N_{\rm WA1}\,(\,{\rm cm}^{-2}\,)$	$1.51^{+0.37}_{-0.12}\times10^{23}$
	$\log\xi_{\rm WA1}$	$2.97^{+0.26}_{-0.04}$
WA 2	$N_{\rm WA2}\,(\,{\rm cm}^{-2}\,)$	$2.90^{+0.30}_{-0.22}\times10^{22}$
	$\log\xi_{\rm WA2}$	$1.24^{+0.05}_{-0.02}$
po	$\Gamma_{\rm po}$	$2.25^{+0.05}_{-0.05}$
	flux $(\,{\rm ph\,cm^{-2}\,s^{-1}}\,)$	$1.27^{+0.04}_{-0.01}\times10^{-4}$
bbody	$kT\,(\,{\rm keV}\,)$	$0.14^{+0.01}_{-0.01}$
	flux $(\,{\rm ph\,cm^{-2}\,s^{-1}}\,)$	$1.95^{+0.04}_{-0.06}\times10^{-6}$
zgauss	E $(\,{\rm keV}\,)$	6.40
	flux $(\,{\rm ph\,cm^{-2}\,s^{-1}}\,)$	$1.15^{+0.23}_{-0.14}\times10^{-7}$
	EW $(\,{\rm eV}\,)$	$54.40^{+10.88}_{-6.62}$
zgauss	E $(\,{\rm keV}\,)$	6.97
	flux $(\,{\rm ph\,cm^{-2}\,s^{-1}}\,)$	$5.40^{+1.69}_{-1.64}\times10^{-8}$
	EW $(\,{\rm eV}\,)$	$19.90^{+6.23}_{-6.04}$
kerrconv	α_1	$2.34^{+0.11}_{-0.05}$
	α_2	$2.34^{+0.11}_{-0.05}$
	$r_{\rm br}\,(r_{\rm ms})$	6.0
	a	$0.65^{+0.03}_{-0.02}$
	$i\,(^\circ)$	79^{+1}_{-0}
	$r_{\rm min}\,(r_{\rm ms})$	<1.09
	$r_{\rm max}\,(r_{\rm ms})$	400
reflion	Fe/solar	1.0
	$\xi_{\rm refl}\,(\,{\rm erg\,cm^{-1}\,s^{-1}}\,)$	30.0
	$\Gamma_{\rm refl}$	$2.25^{+0.05}_{-0.05}$
	$R_{\rm refl}$	$2.17^{+1.06}_{-0.05}$
	flux $(\,{\rm ph\,cm^{-2}\,s^{-1}}\,)$	$4.03^{+1.96}_{-0.10}\times10^{-7}$
χ^2/dof		1543/1421 (1.09)

Table 11: Best-fitting model parameters for the 2.5 – 10.0 keV spectrum of Ark 120, including components and parameter values from 0.6 – 1.5 keV for completeness. The energies from 1.5 – 2.5 keV were not included due to the presence of absorption edges from the *XMM-Newton* mirrors. Error bars are quoted at 90% confidence. We required the zgauss lines to be intrinsically narrow, i.e., $\sigma = 0.0$. Redshifts were frozen at the cosmological value for the source, in this case $z = 0.0327$. A two-zone warm absorber and blackbody soft excess are present in this object, as in many other Sy-1 sources.

ration of ~ 29 ks ($\sim 3.95 \times 10^5$ photons) (Jansen et al. 2001), and the EPIC-pn data were presented in full by Gondoin et al. the following year (Gondoin et al. 2001). We have followed the general procedures for data reduction and analysis discussed by Gondoin et al., using the most up-to-date calibration files and software as we have for all other sources analyzed in this work.

Gondoin et al. find that continuum of Fairall 9 is best modeled with a photoabsorbed power-law ($N_{\rm H} = 3 \times 10^{20}\,{\rm cm}^{-2}$, $\Gamma = 1.80$), in which the absorbing column density of neutral hydrogen gas is approximately equal to its Galactic value along the line of sight to this source ($N_{\rm H} = 3.19 \times 10^{20}\,{\rm cm}^{-2}$). A soft excess is noted below ~ 2 keV, and an RGS analysis yielded a best-fitting blackbody model for this component: $kT = 0.17$ keV. Incorporating reflection from an ionized disk with solar abundances and a reflection fraction of $f_{\rm refl} = 1.0$, the authors find that the high-energy tail is quite well modeled by a disk at an inclination angle of $i = 26°$ (Gondoin et al. 2001). We have performed a similar fit using only the EPIC-pn data, and find some similar parameters describing the power-law, blackbody soft excess and reflection components (the column density of neutral hydrogen absorption was frozen at the Galactic value): $\Gamma = 2.04$, $kT = 0.20$ keV with a flux $\sim 0.5\%$ that of the power-law component, and the disk inclination angle is $i = 57°$ for solar abundance and assumed near-neutrality. Unfortunately, due to the relatively small number of photons, the disk ionization and metallicity were not able to be adequately constrained, hence the assumptions of solar metallicity and near-neutrality. In contrast to the Gondoin et al. analysis, we do detect evidence for a warm absorber within the system with $N_{\rm WA} = 1.21 \times 10^{23}\,{\rm cm}^{-2}$ and $\log \xi_{\rm WA} = 2.85$. Inclusion of this component improves the global goodness-of-fit by $\Delta\chi^2/{\rm dof} = -13/+2$, making it statistically significant according to the F-test. The presence of the warm absorber also eliminates some of the residual continuum curvature in the soft spectrum.

Gondoin et al. also note the presence of a 6.4 keV Fe-Kα line in the spectrum with $EW \sim 120$ eV, which they modeled with a Gaussian component. Due to its relatively narrow profile, the line is suggested to originate from low-ionization material orbiting relatively far out in the disk. Additionally, an Fe-K absorption edge is also noted at 7.64 keV with $\tau = 0.18$, consistent with reflection from cold, optically thick material. We find that the inclusion of such an edge is not statistically robust in our model once reflection is included, but we do find the 6.4 keV line in emission and model it first with a narrow Gaussian feature representing the core of the Fe-Kα line. This feature has an $EW = 133$ eV, but even after its inclusion residual features remain indicating the presence of a broader iron line component. The best fit for this line, which is physically consistent with our disk reflection model, is achieved using a `kerrconv(refl)` component with an inner radius of emission of $r_{\rm min} < 6.27\,r_{\rm ms}$, or $< 10.75\,r_{\rm g}$, calculated using the fit value of BH spin ($a = 0.972$). The BH spin itself, however, was unable to be constrained. Best-fit values and error bars for all the parameters in our model are listed in Table 12. Fig. 9 shows the iron line residual, best fit to this residual, and relative contributions of the individual model components, respectively.

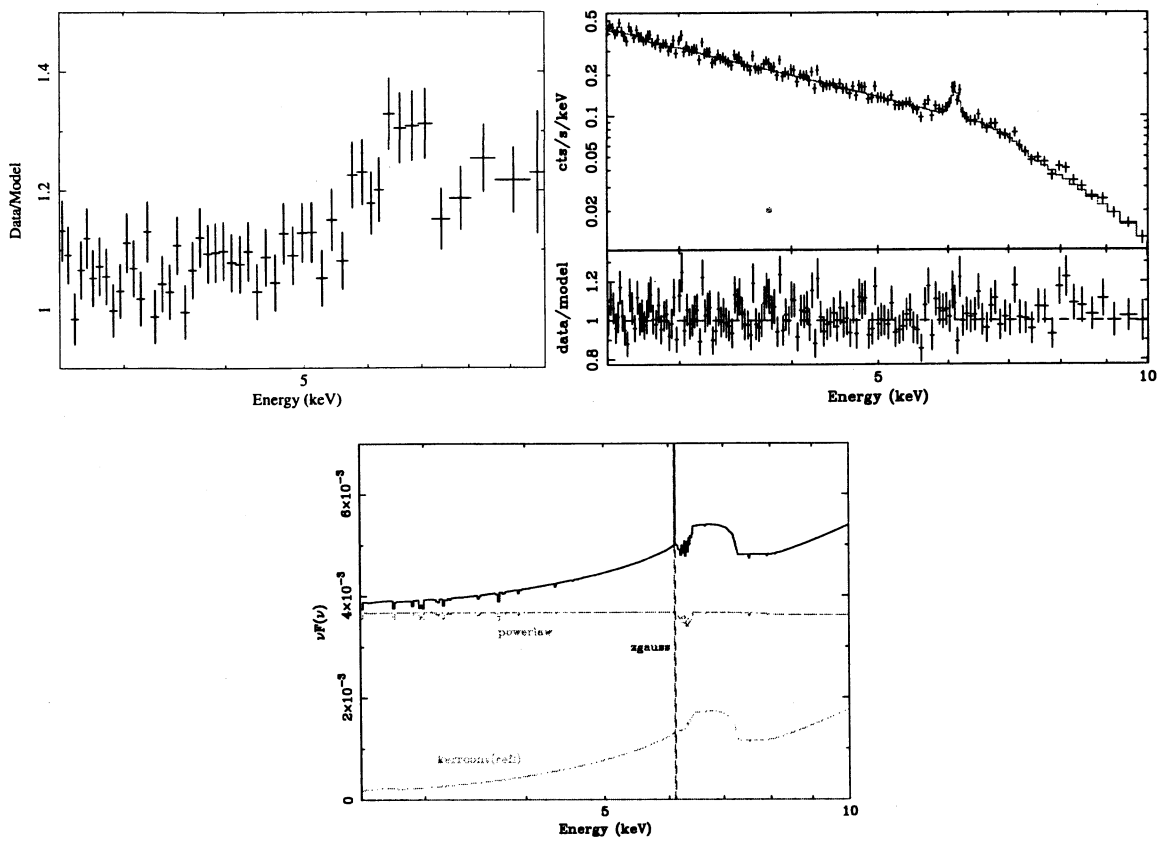

Fig. 9.— *Top left:* The 2.5 – 10.0 keV spectrum of Fairall 9 fit with a continuum composed of a power-law model modified by Galactic photoabsorption, a warm absorber model and a blackbody soft excess. *Top right:* The 2.5 – 10.0 keV best-fit model for Fairall 9, including our continuum model and an ionized disk reflection spectrum convolved with our `kerrconv` relativistic smearing kernel. *Bottom:* A νF_ν plot depicting the relative flux in each of the model components in the spectrum.

Model Component	Parameter	Value
phabs	$N_{\rm H}\,(\rm cm^{-2})$	$3.19^{+0.42}_{-0.00} \times 10^{20}$
WA	$N_{\rm WA}\,(\rm cm^{-2})$	$1.21^{+1.60}_{-0.97} \times 10^{23}$
	$\log \xi_{\rm WA}$	$2.85^{+0.89}_{-0.79}$
po	$\Gamma_{\rm po}$	$2.04^{+0.14}_{-0.10}$
	flux (ph cm^{-2} s^{-1})	$3.28^{+0.47}_{-0.30} \times 10^{-4}$
bbody	kT (keV)	$0.20^{+0.01}_{-0.02}$
	flux (ph cm^{-2} s^{-1})	$1.57^{+0.40}_{-0.35} \times 10^{-6}$
zgauss	E (keV)	6.40
	flux (ph cm^{-2} s^{-1})	$1.16^{+0.42}_{-0.27} \times 10^{-6}$
	EW (eV)	133^{+48}_{-31}
kerrconv	α_1	$5.17^{+4.83}_{-3.31}$
	α_2	$5.17^{+4.83}_{-3.31}$
	$r_{\rm br}\,(r_{\rm ms})$	6.0
	a	– – –
	$i\,(^\circ)$	57^{+7}_{-5}
	$r_{\rm min}\,(r_{\rm ms})$	< 6.27
	$r_{\rm max}\,(r_{\rm ms})$	400
reflion	Fe/solar	1.0
	$\xi_{\rm refl}$ (erg cm^{-1} s^{-1})	30.0
	$\Gamma_{\rm refl}$	$2.04^{+0.14}_{-0.10}$
	$R_{\rm refl}$	$2.63^{+1.37}_{-0.87}$
	flux (ph cm^{-2} s^{-1})	$8.10^{+4.21}_{-2.66} \times 10^{-7}$
χ^2/dof		665/691 (0.96)

Table 12: Best-fitting model parameters for the 2.5 – 10.0 keV spectrum of Fairall 9, including components and parameter values from 0.6 – 1.5 keV for completeness. The energies from 1.5 – 2.5 keV were not included due to the presence of absorption edges from the *XMM-Newton* mirrors. Error bars are quoted at 90% confidence. We required the 6.4 keV zgauss line to be intrinsically narrow, i.e., $\sigma = 0.0$. Redshifts were frozen at the cosmological value for the source, in this case $z = 0.0470$. A warm absorber and blackbody soft excess are present in this object, as in many other Sy-1 sources.

REFERENCES

Balestra, I., Bianchi, S., & Matt, G. 2004, *Astr. Astrophys.*, 415, 437

Behar, E., Rasmussen, A. P., Blustin, A. J., Sako, M., Kahn, S. M., Kaastra, J. S., Branduardi-Raymont, G., & Steenbrugge, K. C. 2003, *Astrophys. J.*, 598, 232

Bevington, P. R. 1969, Data reduction and error analysis for the physical sciences (New York: McGraw-Hill, 1969)

Blustin, A. J., Branduardi-Raymont, G., Behar, E., Kaastra, J. S., Kahn, S. M., Page, M. J., Sako, M., & Steenbrugge, K. C. 2002, *Astr. Astrophys.*, 392, 453

Brandt, W. N., Fabian, A. C., Nandra, K., & Tsuruta, S. 1993, *Mon. Not. R. astr. Soc.*, 265, 996

Brenneman, L. W. & Reynolds, C. S. 2006, *Astrophys. J.*, 652, 1028

Crenshaw, D. M. & Kraemer, S. B. 2001, *Astrophys. J. Lett.*, 562, L29

Crenshaw, D. M., Kraemer, S. B., Boggess, A., Maran, S. P., Mushotzky, R. F., & Wu, C.-C. 1999, *Astrophys. J.*, 516, 750

Dewangan, G. C., Griffiths, R. E., & Schurch, N. J. 2003, *Astrophys. J.*, 592, 52

Edelson, R. A. & Malkan, M. A. 1986, *Astrophys. J.*, 308, 59

Fabian, A. C., Vaughan, S., Nandra, K., Iwasawa, K., Ballantyne, D. R., Lee, J. C., de Rosa, A., Turner, A., & Young, A. J. 2002, *Mon. Not. R. astr. Soc.*, 335, L1

George, I. M., Turner, T. J., Mushotzky, R., Nandra, K., & Netzer, H. 1998, *Astrophys. J.*, 503, 174

George, I. M., Turner, T. J., & Netzer, H. 1995, *Astrophys. J. Lett.*, 438, L67

Gilli, R., Maiolino, R., Marconi, A., Risaliti, G., Dadina, M., Weaver, K. A., & Colbert, E. J. M. 2000, *Astr. Astrophys.*, 355, 485

Gondoin, P., Lumb, D., Siddiqui, H., Guainazzi, M., & Schartel, N. 2001, *Astr. Astrophys.*, 373, 805

Guainazzi, M., Bianchi, S., & Dovčiak, M. 2006, Astronomische Nachrichten, 327, 1032

Guainazzi, M., Mihara, T., Otani, C., & Matsuoka, M. 1996, *Publ. astr. Soc. Japan*, 48, 781

Haardt, F., Fossati, G., Grandi, P., Celotti, A., Pian, E., Ghisellini, G., Malizia, A., Maraschi, L., Paciesas, W., Raiteri, C. M., Tagliaferri, G., Treves, A., Urry, C. M., Villata, M., & Wagner, S. 1998, *Astr. Astrophys.*, 340, 35

Jansen, F., Lumb, D., Altieri, B., Clavel, J., Ehle, M., Erd, C., Gabriel, C., Guainazzi, M., Gondoin, P., Much, R., Munoz, R., Santos, M., Schartel, N., Texier, D., & Vacanti, G. 2001, *Astr. Astrophys.*, 365, L1

Kaspi, S., Brandt, W. N., George, I. M., Netzer, H., Crenshaw, D. M., Gabel, J. R., Hamann, F. W., Kaiser, M. E., Koratkar, A., Kraemer, S. B., Kriss, G. A., Mathur, S., Mushotzky, R. F., Nandra, K., Peterson, B. M., Shields, J. C., Turner, T. J., & Zheng, W. 2002, *Astrophys. J.*, 574, 643

Kaspi, S., Brandt, W. N., Netzer, H., George, I. M., Chartas, G., Behar, E., Sambruna, R. M., Garmire, G. P., & Nousek, J. A. 2001, *Astrophys. J.*, 554, 216

Kaspi, S., Brandt, W. N., Netzer, H., Sambruna, R., Chartas, G., Garmire, G. P., & Nousek, J. A. 2000, *Astrophys. J. Lett.*, 535, L17

Kataoka, J., Tanihata, C., Kawai, N., Takahara, F., Takahashi, T., Edwards, P. G., & Makino, F. 2002, *Mon. Not. R. astr. Soc.*, 336, 932

King, A. R., Pringle, J. E., & Hofmann, J. A. 2008, ArXiv e-prints, 801

Lamer, G., McHardy, I. M., Uttley, P., & Jahoda, K. 2003, *Mon. Not. R. astr. Soc.*, 338, 323

Leighly, K. M., Mushotzky, R. F., Yaqoob, T., Kunieda, H., & Edelson, R. 1996, *Astrophys. J.*, 469, 147

Mason, K. O., Branduardi-Raymont, G., Ogle, P. M., Page, M. J., Puchnarewicz, E. M., Behar, E., Córdova, F. A., Davis, S., Maraschi, L., McHardy, I. M., O'Brien, P. T., Priedhorsky, W. C., & Sasseen, T. P. 2003, *Astrophys. J.*, 582, 95

Mason, K. O., McHardy, I. M., Page, M. J., Uttley, P., Córdova, F. A., Maraschi, L., Priedhorsky, W. C., Puchnarewicz, E. M., & Sasseen, T. 2002, *Astrophys. J. Lett.*, 580, L117

Matt, G., Perola, G. C., Fiore, F., Guainazzi, M., Nicastro, F., & Piro, L. 2000, *Astr. Astrophys.*, 363, 863

McHardy, I. M., Lawrence, A., Pye, J. P., & Pounds, K. A. 1981, *Mon. Not. R. astr. Soc.*, 197, 893

Miller, J. M. 2007, ArXiv e-prints, 705

Nandra, K., George, I. M., Mushotzky, R. F., Turner, T. J., & Yaqoob, T. 1997, *Astrophys. J.*, 476, 70

Nandra, K., O'Neill, P. M., George, I. M., & Reeves, J. N. 2007, MNRAS, 382, 194

Narayan, R., McClintock, J. E., & Shafee, R. 2007, ArXiv e-prints, 710

Nordgren, T. E., Helou, G., Chengalur, J. N., Terzian, Y., & Khachikian, E. 1995, *Astrophys. J. Suppl.*, 99, 461

Page, K. L., Turner, M. J. L., Done, C., O'Brien, P. T., Reeves, J. N., Sembay, S., & Stuhlinger, M. 2004, *Mon. Not. R. astr. Soc.*, 349, 57

Piccinotti, G., Mushotzky, R. F., Boldt, E. A., Holt, S. S., Marshall, F. E., Serlemitsos, P. J., & Shafer, R. A. 1982, *Astrophys. J.*, 253, 485

Ponti, G., Miniutti, G., Cappi, M., Maraschi, L., Fabian, A. C., & Iwasawa, K. 2006, *Mon. Not. R. astr. Soc.*, 368, 903

Pounds, K. A., Nandra, K., Fink, H. H., & Makino, F. 1994, *Mon. Not. R. astr. Soc.*, 267, 193

Pounds, K. A., Reeves, J. N., King, A. R., & Page, K. L. 2004, *Mon. Not. R. astr. Soc.*, 350, 10

Pounds, K. A., Reeves, J. N., Page, K. L., Wynn, G. A., & O'Brien, P. T. 2003, *Mon. Not. R. astr. Soc.*, 342, 1147

Reeves, J. N., Awaki, H., Dewangan, G. C., Fabian, A. C., Fukazawa, Y., Gallo, L., Griffiths, R., Inoue, H., Kunieda, H., Markowitz, A., Miniutti, G., Mizuno, T., Mushotzky, R., Okajima, T., Ptak, A., Takahashi, T., Terashima, Y., Ushio, M., Watanabe, S., Yamasaki, T., Yamauchi, M., & Yaqoob, T. 2007, *Publ. astr. Soc. Japan*, 59, 301

Reeves, J. N., Fabian, A. C., Kataoka, J., Kunieda, H., Markowitz, A., Miniutti, G., Okajima, T., Serlemitsos, P., Takahashi, T., Terashima, Y., & Yaqoob, T. 2006, Astronomische Nachrichten, 327, 1079

Reeves, J. N., Nandra, K., George, I. M., Pounds, K. A., Turner, T. J., & Yaqoob, T. 2004, *Astrophys. J.*, 602, 648

Reynolds, C. S. 1997, *Mon. Not. R. astr. Soc.*, 236, 513

Reynolds, C. S. & Nowak, M. A. 2003, *Phys. Reports*, 377, 389

Ross, R. R. & Fabian, A. C. 2005, *Mon. Not. R. astr. Soc.*, 358, 211

Ross, R. R., Fabian, A. C., & Brandt, W. N. 1996, *Mon. Not. R. astr. Soc.*, 278, 1082

Schurch, N. J., Warwick, R. S., Griffiths, R. E., & Kahn, S. M. 2004, *Mon. Not. R. astr. Soc.*, 350, 1

Sikora, M., Stawarz, Ł., & Lasota, J.-P. 2007, *Astrophys. J.*, 658, 815

Türler, M., Chernyakova, M., Courvoisier, T. J.-L., Foellmi, C., Aller, M. F., Aller, H. D., Kraus, A., Krichbaum, T. P., Lähteenmäki, A., Marscher, A., McHardy, I. M., O'Brien, P. T., Page, K. L., Popescu, L., Robson, E. I., Tornikoski, M., & Ungerechts, H. 2006, *Astr. Astrophys.*, 451, L1

Turner, M. J. L., Williams, O. R., Courvoisier, T. J. L., Stewart, G. C., Nandra, K., Pounds, K. A., Ohashi, T., Makishima, K., Inoue, H., Kii, T., Makino, F., Hayashida, K., Tanaka, Y., Takano, S., & Koyama, K. 1990, *Mon. Not. R. astr. Soc.*, 244, 310

Turner, T. J., Kraemer, S. B., George, I. M., Reeves, J. N., & Bottorff, M. C. 2005, *Astrophys. J.*, 618, 155

Turner, T. J., Miller, L., George, I. M., & Reeves, J. N. 2006, *Astr. Astrophys.*, 445, 59

Turner, T. J., Nandra, K., George, I. M., Fabian, A. C., & Pounds, K. A. 1993, *Astrophys. J.*, 419, 127

Turner, T. J. & Pounds, K. A. 1989, *Mon. Not. R. astr. Soc.*, 240, 833

Uttley, P., Fruscione, A., McHardy, I., & Lamer, G. 2003, *Astrophys. J.*, 595, 656

Uttley, P., Taylor, R. D., McHardy, I. M., Page, M. J., Mason, K. O., Lamer, G., & Fruscione, A. 2004, *Mon. Not. R. astr. Soc.*, 347, 1345

Vaughan, S., Fabian, A. C., Ballantyne, D. R., De Rosa, A., Piro, L., & Matt, G. 2004, *Mon. Not. R. astr. Soc.*, 351, 193

Volonteri, M., Madau, P., Quataert, E., & Rees, M. J. 2005, *Astrophys. J.*, 620, 69

Wandel, A., Peterson, B. M., & Malkan, M. A. 1999, *Astrophys. J.*, 526, 579

Ward, M., Elvis, M., Fabbiano, G., Carleton, N. P., Willner, S. P., & Lawrence, A. 1987, *Astrophys. J.*, 315, 74

Weaver, K. A., Krolik, J. H., & Pier, E. A. 1998, *Astrophys. J.*, 498, 213

Weaver, K. A., Yaqoob, T., Mushotzky, R. F., Nousek, J., Hayashi, I., & Koyama, K. 1997, *Astrophys. J.*, 474, 675

Yaqoob, T. & Serlemitsos, P. 2000, *Astrophys. J. Lett.*, 544, L95